1 **Structure of dual-BON domain protein DolP identifies phospholipid binding as**

2 **a new mechanism for protein localization**

3

4 J. A. Bryant[1†], F. C. Morris[1†], T. J. Knowles[1,2†], R. Maderbocus[1,3], E. Heinz[5*], G.

5 Boelter[1], D. Alodaini[1], A. Colyer[1], P. J. Wotherspoon[1], K. A. Staunton[1], M. Jeeves[3],

6 D. F. Browning[1], Y. R. Sevastsyanovich[1], T. J. Wells[1], A. E. Rossiter[1], V. N. Bavro[1],

7 P. Sridhar[2], D. G. Ward[2], Z-S. Chong[6], E. C. A. Goodall[1,7], C. Icke[1,7], A. Teo[8], S-S.

8 Chng[6], D. I. Roper[8], T. Lithgow[5], A. F. Cunningham[1,4], M. Banzhaf[1], M. Overduin[2,9†],

9 I. R. Henderson[1,6†]

10

11 [1]Institute of Microbiology and Infection, [2]School of Biosciences, [3]Institute for Cancer

12 and Genomic Sciences, and [4]Institute of Inflammation and Immunotherapy,

13 University of Birmingham, Edgbaston, U.K. [5]Infection & Immunity Program,

14 Biomedicine Discovery Institute and Department of Microbiology, Monash University,

15 Clayton, Australia. [6]Department of Chemistry, National University of Singapore,

16 Singapore. [7]Institute for Molecular Bioscience, University of Queensland, St. Lucia,

17 Australia. [8]School of Life Sciences, The University of Warwick, Coventry, U.K.

18 [9]Department of Biochemistry, University of Alberta, Edmonton, AB T6G 2H7,

19 Canada.

20

21 *now located at Liverpool School of Tropical Medicine, Department of Vector

22 Biology, Liverpool L3 5QA, UK.

23

24 **Correspondence should be addressed to I.R.H. (i.henderson@uq.edu.au)**

25 [†]These authors contributed equally to this work

26

Abstract

The Gram-negative outer membrane envelops the bacterium and functions as a permeability barrier against antibiotics, detergents and environmental stresses. Some virulence factors serve to maintain the integrity of the outer membrane, including DolP (formerly YraP) a protein of unresolved structure and function. Here we reveal DolP is a lipoprotein functionally conserved among Gram-negative bacteria and that loss of DolP increases membrane fluidity. We present the NMR solution structure for *Escherichia coli* DolP, which is composed of two BON domains that form an interconnected opposing pair. The C-terminal BON domain binds anionic phospholipids through an extensive membrane:protein interface. This interaction is essential for DolP function and is required for sub-cellular localization of the protein to the cell division site, providing evidence of subcellular localization of these phospholipids within the outer membrane. The structure of DolP provides a new target for developing therapies that disrupt the integrity of the bacterial cell envelope.

Significance

BON domain proteins are conserved in all Gram-negative bacteria. Here we reveal DolP, a BON domain protein required for the maintenance of outer membrane integrity, is functionally conserved across Gram-negative bacteria. We present the first structure of a dual BON domain protein revealing the C-terminal BON domain interfaces anionic phospholipid and illustrating a novel mechanism of lipid binding. We demonstrate that interaction with phospholipids is essential for DolP function and is required for subcellular localization of the protein to the division site. To our knowledge, this represents the first example of this mechanism of localization to the bacterial division site. Our data provides the first evidence that anionic phospholipids localize to sites of high membrane curvature in the outer membrane.

Introduction

Gram-negative bacteria are intrinsically resistant to many antibiotics and environmental insults, which is largely due to the presence of their hydrophobic outer membrane (OM). This asymmetric bilayer shields the periplasmic space, a thin layer of peptidoglycan and the inner membrane (IM). In the model bacterium *Escherichia coli,* the IM is a symmetrical phospholipid bilayer, whereas the OM has a more complex organization with lipopolysaccharide (LPS) and phospholipids forming an asymmetric bilayer containing integral β-barrel proteins [1,2]. The OM is also decorated with lipoproteins (approximately 75 have been identified in *E. coli*), many of which, are functional orphans [3,4]. Biogenesis of the OM is completed by several proteinaceous systems, which must bypass the periplasmic, mesh-like peptidoglycan [2,5-7]. The growth of all three envelope layers must be tightly coordinated in order to maintain membrane integrity. Improper coordination can lead to bacterial growth defects, sensitivity to antibiotics, and can cause cell lysis [5,8].

DolP (**d**ivision and **O**M stress-associated **l**ipid-binding **p**rotein; formerly YraP) is a nonessential protein found in *E. coli* and other Gram-negative bacteria [9]. Loss of DolP results in the disruption of OM integrity, induces increased susceptibility to detergents and antibiotics, and attenuates the virulence of *Salmonella enterica* [10]. Importantly, DolP is a crucial component of the serogroup B meningococcal vaccine where it enhances the immunogenicity of other components by an unknown mechanism [11]. Recently, the *dolP* gene was connected genetically to the activation of peptidoglycan amidases during *E. coli* cell division, however this activity has not been directly confirmed experimentally [12]. In contrast, protein interactome studies suggest DolP is a component of the β-barrel assembly machine (Bam) complex [13,14]. While these data suggest that DolP may be involved in outer membrane protein (OMP) biogenesis and the regulation of peptidoglycan remodeling, its precise function in either of these processes remained unclear. Nonetheless, given its roles in these vital cell envelope processes, and its requirement for virulence and the maintenance of cell envelope integrity, DolP is a potential target for the development of therapeutics.

In this study, we demonstrate that DolP is an outer membrane lipoprotein functionally conserved amongst Gram-negative bacteria, but with a function distinct from other

BON (Bacterial OsmY and nodulation) domain containing proteins. We solve the NMR solution structure of DolP revealing the first view of a dual-BON domain fold. Extensive structural and functional analyses define a membrane:protein interface that binds DolP to anionic phospholipids and provides the basis for a new mechanism for targeting proteins to the cell division site. We show that loss of *dolP* affects OM fluidity, which perturbs the BAM complex, suggesting an indirect role for DolP in OMP biogenesis. The insights provided here not only advance our understanding of how DolP functions but provide a basis for beginning to develop drugs to target it.

Results

DolP belongs to an extensive family of lipoproteins required for OM homeostasis

In *E. coli,* the *dolP* gene is located downstream of the genes encoding LpoA (an activator of PBP1A) [15], YraN (a putative Holiday-Junction resolvase), and DiaA (a regulator of chromosomal replication) [16], and two σ^E-dependent promoters are found immediately upstream of the *dolP* gene [17] **(Figure 1A)**. Bioinformatic analyses predicted that *dolP* encodes a lipoprotein with two putative domains of unknown function, termed BON domains [18], as well as a Lol-dependent OM targeting signal sequence where acylation was predicted to occur on cysteine residue C19. To test the hypothesis that DolP is localized to the periplasmic face of the OM, we raised an antiserum to the protein to probe subcellular fractions. DolP was found in the Triton X-100 insoluble fraction of the *E. coli* cell envelope along with other OM proteins. As a control for the antiserum, DolP was absent from Triton X-100 insoluble fractions of cell envelopes harvested from *E. coli* Δ*dolP* **(Figure 1-figure supplement 1A)**. Furthermore, expression of a C19A point mutant, preventing N-terminal acylation, effectively eliminated DolP from the OM fractions **(Figure 1-figure supplement 1B).** Unlike the lipoproteins BamC and Lpp, which can be surface localized [19,20], DolP was not accessible to antibody or protease in intact *E. coli* cells. However, DolP could be labelled and degraded when OM integrity was compromised **(Figure 1-figure supplement 1C,D)**, confirming that DolP is predominantly targeted to the inner leaflet of the OM, localizing it within the periplasmic space.

Further in silico analyses revealed the DolP lipoprotein was conserved across diverse species of Proteobacteria and is present even in organisms with highly-reduced genomes e.g. *Buchnera* spp **(Table 1 and Supplementary file 1).** The genome of *E. coli* contains three BON domain-containing proteins: DolP, OsmY and Kbp. DolP shares a dual BON-domain architecture and 29.5% sequence identity with OsmY, which is distinguished from DolP by a canonical Sec-dependent signal sequence. In contrast, Kbp consists of single BON and LysM domains and lacks a discernible signal sequence **(Figure 1A)**. Our comprehensive analysis found seven predominant domains co-occurring with BON in different modular protein architectures across bacterial phyla, suggesting specialized roles for BON domains **(Table 1 and Figure 1-figure supplement 2)**. Clustering analyses of sequences obtained by HMMER searches revealed DolP, OsmY and Kbp are distributed throughout the α, β and γ-proteobacteria and form distinct clusters indicating that DolP has a role that is independent of OsmY and Kbp **(Figure 1B).** Our analyses demonstrated that OsmY and Kbp are not functionally redundant with DolP and isogenic mutants show distinct phenotypes, therefore confirming a distinct role for DolP in *E. coli* **(Figure 1-figure supplement 3).**

Previously, we demonstrated that loss of *dolP* in *S. enterica* conferred susceptibility to vancomycin and SDS, suggesting DolP plays an important role in maintaining the integrity of the OM [10]. Further evidence of a role for DolP in maintaining OM integrity is shown by *E. coli* Δ*dolP* susceptibility to vancomycin, SDS, cholate, and deoxycholate **(Figure 1C and Figure 1-figure supplement 4A).** Resistance could be restored by supplying *dolP* in *trans* **(Figure 1C)**. Despite evidence for disrupted OM integrity, the growth rate observed for the *dolP* mutant strain was identical to that of the parent, and scanning-electron microscopy revealed no obvious differences in cell size or shape **(Figure 1-figure supplement 4B,C)**. To determine whether DolP is broadly required for OM homeostasis, plasmids expressing DolP homologues from *S. enterica*, *Vibrio cholerae*, *Pasteurella multocida*, *Haemophilus influenza* and *Neisseria meningitidis* were shown to restore the OM barrier function of the *E. coli* Δ*dolP* mutant **(Figure 1F)**. Finally, either replacement of the DolP signal sequence with that of PelB[12], which targets the protein to the periplasmic space, or mutation of the signal sequence to avoid OM targeting *via* the Lol system, prevented complementation of the Δ*dolP* phenotype **(Figure 1-figure supplement 5)**. Together these results support a conserved role for DolP in maintenance of OM integrity

160 throughout Gram-negative bacteria and demonstrate that localization of DolP to the
161 inner leaflet of the OM is essential to mediate this function.

162

163 *The structure of DolP reveals a dual-BON domain lipoprotein*

164

165 To gain further insight into the function of DolP, the structure of full-length mature *E.*
166 *coli* DolP was determined by NMR spectroscopy. To promote native folding of DolP,
167 the protein was over-expressed in the periplasm using a PelB signal sequence; the
168 N-terminal cysteine was removed to prevent acylation and provide for rapid
169 purification of the soluble protein. Purified DolP was processed, soluble and
170 monomeric, as confirmed by analytical ultra-centrifugation and size exclusion
171 chromatography **(Figure 2-figure supplement 1)**. Using a standard Nuclear
172 Overhauser Effect (NOE)-based approach, a convergent ensemble was calculated
173 from the 20 lowest-energy solution structures, revealing two BON domains facing
174 away from each other and offset by ~45° **(Figure 2A and Figure 2-figure**
175 **supplement 2).** The individual BON1 (Residues 45-112) and BON2 (Residues 114-
176 193) domains have C-alpha backbone root mean square deviations (RMSDs) of 0.3
177 and 0.3 Å, respectively, and an overall global RMSD of 0.5 Å **(Table 2)**. Despite
178 having low sequence identity (24.7%) each BON domain consists of a three-
179 stranded mixed parallel/antiparallel β-sheet packed against two α-helices yielding an
180 αββαβ topology. The two BON domains present high structural homology and
181 superpose with an RMSD of 1.8 Å over C-alpha backbone **(Figure 2-figure**
182 **supplements 2 and 3).** Notably, BON1 is embellished by an additional short α1*
183 helix between BON1:α1 and BON1:β1 **(Figure 2A and Figure 2-figure**
184 **supplements 2 and 3)**. The N-terminal acylation site is connected through a 27
185 amino acid dynamic unstructured linker **(Figure 2B)**. The molecular envelope of full
186 length DolP calculated by small angle X-ray scattering (SAXS) accommodated the
187 NMR derived structure of DolP and supported the presence of a flexible N-terminal
188 extension. The experimentally determined scattering curve fit the NMR derived
189 structure with a χ^2 of 1.263, confirming the accuracy of the NMR-derived structure
190 and an exclusively monomeric state **(Figure 2C and Figure 2-figure supplement**
191 **4)**.

192

193 The two BON domains pack against each other *via* their β-sheets through contacts
194 mediated directly by Y75 and V82 in BON1 and T150, G160, L161 and T188 in

195   BON2 with a total of 38 interdomain NOEs **(Figure 2D, Figure 2-figure supplement**

196   **5, Table 3).** This interdomain orientation is consistent with SAXS analysis **(Figure**

197   **2C)** and appears to be essential for function as the mutation Y75A abolishes function

198   **(Figure 2D).** Single point mutations (G83V and G160V) of the highly conserved

199   glycine residues had less effect, however the double mutant was non-functional

200   **(Figure 2D and Figure 2-figure supplement 3)**. Since the latter protein was not

201   detectable by Western immunoblotting this is likely due to structural instability

202   **(Figure 2D)**.

203

204   The elements of DolP that are required for function were mapped using an unbiased

205   linker-scanning mutagenesis screen. The resulting DolP derivatives, containing in-

206   frame 5-amino-acid insertions, were tested for stability by Western immunoblotting.

207   Functional viability was assessed by their capacity to restore growth of *E. coli* Δ*dolP*

208   in the presence of SDS **(Figure 2E).** Seven mutants occurred in the signal sequence

209   and the linker region and were not considered further. Eight insertions were identified

210   in BON1, with insertions at positions L50 (BON1:α1) and V72 (BON1:β1) failing to

211   complement the Δ*dolP* defect whereas the rest were well tolerated. Five insertions

212   were found in BON2, with those at positions L136, L142 and G160 being well

213   tolerated. The remaining insertions at positions D125 and W127 occurred in

214   BON2:α1 but failed to complement the Δ*dolP* phenotype. None of these mutations

215   abolished protein expression. These data indicate the importance of BON2:α1 in

216   maintaining DolP function and OM integrity **(Figure 2E)**.

217

218   *DolP binds specifically to anionic phospholipids via BON2*

219

220   Given that OM permeability defects are often associated with the loss or modification

221   of molecular partners, we sought to identify DolP ligands. Scrutiny of the literature

222   revealed high-throughput protein:protein interaction data[13,14] indicating that DolP co-

223   located with components of the BAM complex in the OM. As the loss of multiple

224   genes encoding different components of a single pathway can have additive

225   phenotypes, such as decreased fitness, we investigated strains with dual mutations

226   in *dolP* and genes coding the non-essential BAM complex components *bamB* or

227   *bamE*. We observed that simultaneous deletion of *dolP* and *bamB* or *bamE* lead to

228   negative genetic interactions and increased rates of cell lysis **(Figure 3-figure**

229   **supplement 1A,B)**, suggesting a potential interaction. However, despite these

230   genetic interactions, in our hands no significant interaction could be detected
231   between DolP and the BAM complex through immunoprecipitations **(Figure 3-figure**
232   **supplement 1C)** and no significant change in overall OMP levels was observed
233   **(Supplementary file 2 and Figure 3-figure supplement 1D)**. Analyses of purified
234   OM fractions revealed no apparent differences in LPS profiles **(Figure 3-figure**
235   **supplement 2A)**, or phospholipid content **(Figure 3-figure supplement 2B)**
236   between the parent and the *dolP* mutant. No significant increase in hepta-acylated
237   Lipid A was observed in the absence of DolP, indicating that the permeability defect
238   is also not due to loss of OM lipid asymmetry **(Figure 3-figure supplement 2C)**. In
239   contrast, Δ*dolP* cells were found to have an increase in membrane fluidity **(Figure 3-**
240   **figure supplement 2D)** as assessed by staining with the membrane intercalating
241   dye pyrene-decanoic acid (PDA), which undergoes a fluorescence shift upon
242   formation of the excimer, an event which is directly related to membrane fluidity[21].
243   Considering that *bamB* mutants are sensitive to increased membrane fluidity[21], these
244   data suggest that the genetic interaction between *dolP* and *bamE* or *bamB*,
245   observed here, is facilitated indirectly through changes to membrane fluidity on the
246   loss of DolP.

247

248   The *dolP* mutant has changes to membrane fluidity and that BON domains are
249   suggested to bind phospholipids[18], therefore we sought to test whether DolP
250   interacts with phospholipids. A set of potential ligands were screened by chemical
251   shift perturbation (CSP) analysis, including *E. coli* OM lipids embedded in micelles.
252   DolP bound specifically to micelles containing the anionic phospholipids
253   phosphatidylglycerol (PG) and cardiolipin (CL) but not to micelles devoid of PG or
254   CL, or those containing the zwitterionic phospholipid phosphatidylethanolamine (PE)
255   **(Figure 3A, Figure 3-figure supplement 3, Figure 4A)**. Significant CSPs were
256   noted for A74, G120-I128, K131-R133, Q135-L137, V142-S145, I173 and S178-
257   V180. The perturbed residues were mapped to the structure, revealing a single
258   extensive binding site centered on BON2:α1 that was sufficiently large to contact
259   several lipid molecules **(Figure 3A)**. A dissociation constant (K_d) of ~100 mM
260   (monomeric DHPG) was measured **(Figure 3-figure supplement 4)**. No lipid
261   interaction was seen for any BON1 domain residue, emphasizing the specialized role
262   of BON2, which not only differs from DolP BON1, but also from the BON domains of
263   OsmY and Kbp **(Figure 2-figure supplement 3)**. Analysis of the electrostatic
264   surface reveals a large negative surface potential on BON1:α1, which is absent in

265 BON2:α1 and may act to repel BON1 from PG, whilst BON2:α1 uniquely harbors an
266 aromatic residue W127 in the observed PG binding site **(Figure 4-figure**
267 **supplement 1)**.

268

269 As the BON2 domain contained a particularly large PG-specific interaction site, we
270 sought to resolve the micelle-complexed structure of mature DolP. Intermolecular
271 structural restraints were obtained from paramagnetic relaxation enhancements
272 (PRE) obtained by incorporating 5-doxyl spin-labelled phosphatidyl choline (PC) and
273 1,2-dimyristoyl-*sn*-glycero-3-phospho-(1'-rac-glycerol)   (DMPG)   into   a   *n*-
274 dodecylphosphocholine (DPC) micelle and by measuring CSPs. The complexed
275 structure was calculated using HADDOCK[22] with 18 PRE distance restraints and
276 side chains of the 25 chemical shift perturbations, with final refinement in water
277 **(Figure 3B)**. The amino acids G120-T130 and V132-S139 were observed to insert
278 into the micelle interior based on the PRE and CSP data. This reveals an
279 unprecedented burial of the BON2:α1 helix, which spans the entirety of the L119-
280 S139 sequence. The protein-micelle interface buries 1358 ± 316 Å^2 and to our
281 knowledge represents the most extensive structured surface of a membrane:protein
282 interface resolved to date. The surface forms intimate contacts with at least six
283 proximal phospholipid headgroups through an extensive network of highly populated
284 hydrogen bonds and electrostatic interactions. Whilst the side chains of residues
285 G120, S123, W127, T130 and S134 intercalate between the acyl chains, E121,
286 N124, T126, I128, K131, R133 and Q135 buttress the interface **(Figure 3B)**. This
287 element was also functionally important based on our transposon screen **(Figure**
288 **2E)**, and was further confirmed as being essential by directed mutagenesis.
289 Mutations within the PG-binding BON2:α1 disrupt the function of DolP, the most
290 critical of which are W127E and L137E; W127 is located in the center of the binding
291 site that penetrates deep into the core of the PG micelle, and L137 is located at the
292 periphery of the helix **(Figure 3B, Figure 4B and Figure 4-figure supplement 2)**.
293 Not only does mutation of W127 lead to loss of function, but introduction of the
294 W127E mutation was shown to abolish binding of DolP to PG micelles as observed
295 by a loss of CSPs within BON2:α1 **(Figure 4C)**. Notably, the BON2:α1 structure
296 presents an extended α-helix when compared to BON1:α1 **(Figure 2-figure**
297 **supplements 2 and 3)**. The helical extension in BON2:α1 contains the W127
298 anionic phospholipid-binding determinant of DolP. This further implicates W127,

299   which is absent in BON1 and OsmY, in specialization of DolP BON2 for phospholipid

300   binding.

301

302   *Phospholipid binding guides DolP localization to the cell division site*

303

304   DolP binds anionic phospholipid, which demonstrates sub-cellular localization to

305   sites of higher membrane curvature including the cell poles and division site [23-25]. To

306   determine if DolP also shows a preference for such sites, we constructed a plasmid

307   expressing a DolP-mCherry fusion and utilizing fluorescence microscopy we

308   observed DolP localized specifically to the cell division site **(Figure 5A)**. Considering

309   that DolP is non-functional when targeted to the IM **(Figure 1-figure supplement 5)**,

310   we investigated if DolP could still localize to the site of cell division when it was

311   mistargeted to the IM; no septal localization was observed **(Figure 1-figure**

312   **supplement 5)**. Next, we tested whether the phospholipid binding activity is also

313   required for division site localization of DolP. We found that introduction of the

314   W127E mutation, which prevents interaction of DolP with PG/CL micelles, abolished

315   division site localization of DolP **(Figure 5A)**. Considering that W127E not only

316   abolished PG/CL binding, but also division site localization, we concluded that

317   division site localization of DolP was dependent upon binding of DolP to anionic

318   phospholipids, which have previously been shown to be enriched at the division

319   site[24,25].

320

321   To confirm this result we analyzed DolP localization in a strain that lacks all three

322   cardiolipin synthases and is defective for cardiolipin synthesis, which was confirmed

323   by phospholipid extraction and thin layer chromatography **(Figure 5B)**. We observed

324   that DolP localization is perturbed in the CL⁻ strain, with less dividing cells showing

325   localization of DolP to the septum **(Figure 5C)**. These effects are further

326   exacerbated in a strain that does not synthesize the major cell anionic phospholipids

327   phosphatidylglycerol or cardiolipin, as confirmed by phospholipid extraction and thin

328   layer chromatography **(Figure 5B)**. Loss of both phosphatidylglycerol and cardiolipin

329   synthesis worsened the severity of the localization defect with less septal localization

330   and a significant proportion of cells showing mislocalization of DolP to patches at the

331   cell poles **(Figure 5C)**. Taken together these data demonstrate that DolP localization

332   to the division site is dependent upon interaction with anionic phospholipid *via*

333   BON2:α1, and that this interaction and the sub-cellular localization are required for

334   DolP function.

335

Discussion

337

338   We have revealed the first structure of a dual-BON domain protein, a protein

339   architecture that is widely conserved among bacteria and therefore provides insight

340   into a diverse range of proteins acting in different organisms. We also report the first

341   evidence for direct binding of lipids by BON domains. We show that DolP BON2

342   demonstrates specificity for the anionic phospholipids PG and CL, which have

343   previously been shown to localize to sites of higher membrane curvature including

344   the cell poles and division site [23-25]. Interestingly, we detected no phospholipid

345   binding for DolP BON1, which lacks the key W127 phospholipid interaction residue.

346   This key residue is also lacking in the other periplasmic BON domain-containing

347   protein in *E. coli*, OsmY. Thus, we have demonstrated a specialized role for DolP in

348   the cell and our data suggests BON domains are not generalist phospholipid binding

349   domains, as was suggested previously[18].

350

351   Here we show for the first time that localization of DolP to the cell division site is

352   dependent upon recognition of anionic phospholipids by DolP BON2. To our

353   knowledge, this is the only example of this mechanism of localization to the bacterial

354   division site [26]. Considering anionic phospholipids also accumulate at the old pole,

355   the question of how DolP specifically recognizes the division site remains. We

356   hypothesize that DolP prefers the site of higher positive (convex) curvature found

357   only at the inner leaflet of the OM cell division site *in vivo* and in the PG micelles

358   used in this study. Previous evidence has shown that inhibition of cell constriction, by

359   the addition of cephalexin, also prevents DolP localization to future division sites[12].

360   This indicates that DolP may require cell constriction for localization to the division

361   site, therefore lending support to the hypothesis that DolP may recognize membrane

362   curvature. An alternative explanation is that the phospholipid binding mode of DolP

363   may trigger interaction with some as yet unidentified division site localized protein

364   partner, but no obvious candidates are offered by published envelope interactome

365   data[13,14]. Nevertheless, these data reveal that DolP function is dependent on

366   localization to the division site through phospholipid binding and localization to the

367   OM through its N-terminal lipid anchor. The model of DolP localization to the cell

368   division site proposed here also provides some evidence that anionic phospholipids

369   localize to sites of high membrane curvature in the OM. While this has been shown

370   for whole cells[23,25], and the IM through the use of spheroplasts[24], to our knowledge,

371   no such observation has yet been made for the OM directly. Considering that the OM

372   is significantly different from the IM and is depleted of PG and CL by comparison[27]

373   **(Figure 3-figure supplement 2B)**, the localization of these lipids to sites of negative

374   curvature could be further enhanced by the relative scarcity of these lipids in the OM

375   and this warrants further study.

376

377   We have not found a direct mechanism through which DolP maintains OM integrity.

378   No differences in LPS content or OM asymmetry were observed in a *dolP* mutant

379   suggesting DolP does not influence the OM phospholipid recycling Mla pathway or

380   LPS biogenesis. Previous protein:protein interaction studies captured DolP as a near

381   neighbor of two components of the Bam complex, BamD and BamE [13,14]. Consistent

382   with this, *dolP* shows synthetic lethality with the gene encoding the periplasmic

383   chaperone SurA, leading to suggestions of a role for DolP in OMP biogenesis [28-30].

384   However, we were unable to demonstrate a direct interaction between DolP and the

385   BAM complex, and no such interaction has been seen in the extensive studies

386   evaluating the subunit composition and multimeric states of the BAM complex[31-34] or

387   in similar studies in *N. meningitidis*[11]. However, while this is in agreement with the

388   fact that DolP is localized to the division site, whereas the Bam complex is uniformly

389   present across the cell surface[33], it does not rule out potential transient interactions.

390   Previous observations revealed that the OM is a rigid structure [35] that this membrane

391   rigidity stabilizes assembly precincts [33], and that the activity of the BAM complex is

392   sensitive to increases in membrane fluidity[21]. We suggest that the increased

393   membrane fluidity of the *dolP* cells, demonstrated here, provides a challenging

394   environment for assembly precincts to be maintained. We hypothesize that DolP,

395   perhaps through interactions with peptidoglycan amidases[12], might also modulate

396   peptidoglycan remodeling in such a way as to minimize the clash between the

397   periplasmic components of the assembly precinct and the cell wall, which might be

398   exacerbated in regions of high membrane curvature.

399

400   In conclusion, this study reports for the first time the direct binding of lipid by BON

401   domains and a new mechanism of protein division site localization. The indirect link

402   between DolP and the general machinery responsible for outer membrane

biogenesis adds to the recently described role of DolP in the regulation of cell wall amidases during division, therefore potentially placing DolP at the interface between envelope biogenesis processes[12]. The demonstration that loss of DolP increases sensitivity to antibiotics and membrane disrupting agents, in addition to the decrease in virulence *in vivo*, and an increase of the efficacy of the *N. meningitidis* vaccine, suggests DolP will provide a useful starting platform for antimicrobial design based on the disruption to regulation of multiple envelope biogenesis mechanisms [10,36,37].

Materials and Methods

Key Resources Table				
Reagent type (species) or resource	**Designation**	**Source or reference**	**Identifier**	**Additional information**
strain, strain background (*Escherichia coli*)	BL21(DE3)	Invitrogen		T7 express, protein expression strain
strain, strain background (*Escherichia coli*)	BW25113	Datsenko and Wanner, 2000		*rrnB3 ΔlacZ*4787 Δ*phoBR*580 *hsdR*514 Δ(*araBAD*)567 Δ(*rhaBAD*)568 galU95 Δ*endA*9::FRT Δ*uidA*3::*pir*(wt) *recA*1 *rph*-1
strain, strain background (*Escherichia coli*)	BW25113 △*dolP*	This paper		BW25113 with *dolP* deleted

strain, strain background (*Escherichia coli*)	BW25113 △*lpp,*△*rcsF*	This paper		BW25113 with *lpp* and *rcsF* deleted
strain, strain background (*Escherichia coli*)	BW25113 △*lpp,*△*rcsF* ,△*pgsA*	This paper		BW25113 with *lpp, rcsF* and *pgsA* genes deleted
strain, strain background (*Escherichia coli*)	BW25113 △*clsA,*△*clsB,*△*clsC*	This paper		BW25113 with *clsA, clsB* and *clsC* genes deleted
genetic reagent (*E. coli*)	KEIO library	Datsenko and Wanner, 2000		Nonessential genes disrupted in *E. coli* BW25113
recombinant DNA reagent	pKD4	Datsenko and Wanner, 2000	Plasmid	Template for the amplification of a kanamycin resistance cassette flanked by FRT sites.
recombinant DNA reagent	pKD46	Datsenko and Wanner, 2000	Plasmid	Temperature sensitive, low copy number plasmid encoding the Lambda RED recombinase genes under the control of an arabinose inducible promoter
recombinant DNA reagent	pCP20	Datsenko and Wanner, 2000	Plasmid	Temperature sensitive plasmid encoding the FLP recombinase gene
recombinant DNA reagent	pET17b	Novagen	Plasmid	T7 expression vector, AmpR
recombinant DNA reagent	pET17b *dolP*	This paper	Plasmid	pET17b with *dolP* cloned between NdeI and EcoRI
recombinant DNA reagent	pET17b *dolP* TM	This paper	Plasmid	As described above with the *dolP* gene randomly disrupted by Transposon mutations
recombinant DNA reagent	pET17b *dolP STm*	This paper	Plasmid	pET17b with the *S. typhimurium dolP* gene cloned between NdeI and

				HindIII
recombinant DNA reagent	pET17b *dolP H.i*	This paper	Plasmid	pET17b encoding a codon optimised *Haemophilus influenza dolP* homolog
recombinant DNA reagent	pET17b *dolP P.m*	This paper	Plasmid	pET17b encoding a codon optimised *Pasteurella multocida dolP* homolog
recombinant DNA reagent	pET17b *dolP N.m*	This paper	Plasmid	pET17b encoding a codon optimised *Neisseria meningitidis dolP* homolog
recombinant DNA reagent	pET17b *dolP V.c*	This paper	Plasmid	pET17b encoding a codon optimised *Vibrio cholera dolP* homolog
recombinant DNA reagent	pET17b *osmY*	This paper	Plasmid	pET17b encoding a codon optimised *E. coli* K12 *osmY*
recombinant DNA reagent	p(OM)OsmY	This paper	Plasmid	pET17b encoding a codon optimised *E. coli* K12 *osmY* synthesised with the *dolP* signal sequence and acylation site in place of the *osmY* signal sequence
recombinant DNA reagent	pET20b	Novagen	Plasmid	T7 expression vector, AmpR
recombinant DNA reagent	pET20b *dolP*	This paper	Plasmid	pET20b with *dolP* cloned between NdeI and EcoRI
recombinant DNA reagent	pET20b *dolP* PM	This paper	Plasmid	pET20b with *dolP* cloned between NdeI and EcoRI with site directed point mutations at various sites
recombinant DNA reagent	pET20b *wbbL*	This paper	Plasmid	pET20b with *wbbL* gene cloned between NdeI and HindIII
recombinant DNA reagent	pET20b *dolP::mCherry*	This paper	Plasmid	pET20b encoding *dolP* fused to a codon optimised *mCherry* gene via a C-terminal 11-codon flexible linker (GGSSLVPSSDP)

recombinant DNA reagent	pET26b *dolPpelB::mCherry*	This paper	Plasmid	pET26b *dolP::mCherry* with the *dolP* signal sequence replaced with that of *pelB*
recombinant DNA reagent	pET20b *dolPIM::mCherry*	This paper	Plasmid	pET20b *dolP::mCherry* with codon 20 and 22 of *dolP* each mutated to aspartic acid
recombinant DNA reagent	pET20b *dolPW127E::mCherry*	This paper	Plasmid	pET20b *dolP::mCherry* with codon 127 mutated to glutamic acid

422

Bioinformatic analyses. The BON domain profile was obtained from Pfam http://pfam.sanger.ac.uk/[38] and used as input for HMMER (hmmsearch version 3.1)[39] against the Uniprot database (http://www.uniprot.org, release 06032013) with an inclusion cutoff of E = 1 without heuristic filters. Sequence redundancy for clustering analysis was minimized using the UniRef100 resource of representative sequences; clustering was performed with the mclblastline program[40,41] based on the e-value obtained by a BlastP run of all-against-all. Optimal settings for the mcl clustering were manually determined, clustering was performed at an e-value cutoff of 1E-2 and an inflation parameter of 1.2 using the scheme 7 setting implemented in mcl. The resulting clusters were matched back to the proteins originally recovered by the HMMER search, and the number of proteins, as well as the number of matched organisms, are summarized for each phylum or subphylum in **Table 1**. UniProt accession numbers of all proteins according to their clusters are given in **Supplementary file 1**. The domain annotation was obtained from the InterPro database[41]. For cluster representation **(Figure 1)**, the program CLANS[42] was used under the default settings. Clusterings with CLANS was based on a subset of OsmY-, DolP- and Kbp-like proteins identified as described above; the respective accession numbers are given in **Table 4**. Pairwise alignment similarity values were analysed at the Protein Information Resource site (PIR; http://pir.georgetown.edu/).

442

Plasmids, bacterial strains and culture conditions. *E. coli* BW25113 was the parental strain used for most investigations. *E. coli dolP::kan*, *osmY::kan* and *kbp::kan* mutants were obtained from the KEIO library[43] and the mutations transduced into a clean parental strain. *E. coli Δ dolP* was created by resolving the Kan^R cassette, as previously described[44]. *E. coli* BW25113 *ΔpgsA* was constructed

448   first by transfer of the *rcsF::aph* allele from the Keio library into *E. coli* BW25113 and

449   removal of the kan^R cassette. The *lpp:aph* allele was then introduced into the $\Delta rcsF$

450   strain and the cassette removed by the λ-Red recombination method of Datsenko

451   and Wanner, due to the presence of Lpp being toxic in the absence of

452   phosphatidylglycerol[44-46]. Finally, the same method was utilized to create the $\Delta pgsA$

453   strain ($\Delta rcsF,\Delta lpp,\Delta pgsA$) The genes encoding DolP and OsmY were amplified from

454   *E. coli* BW25113 and cloned into pET17b to create pDolP and pOsmY. Orthologous

455   sequences from *S. enterica, V. cholera, N. meningitidis, H. influenza* and *P.*

456   *multocida* were synthesized and cloned into pET17b to create the plasmids pSe,

457   pVc, pNm, pHi and pPm, respectively. To create pDolP^{pelB}, the gene encoding DolP

458   was synthesized but with nucleotides encoding the PelB signal sequence in place of

459   the native signal sequence and without Cys19 to relieve the possibility of acylation;

460   this plasmid was constructed in pET26b+ such that the protein had a C-terminal His-

461   tag. In addition, to create p(OM)OsmY the gene encoding OsmY was synthesized

462   but with nucleotides encoding the native DolP signal sequence and Cys19 N-

463   terminal acylation site in place of the native OsmY signal sequence. The latter

464   plasmid was constructed in pET17b. The pET17b-*dolP::mCherry* plasmid was

465   constructed to contain an 11 amino acid flexible linker and a codon optimized

466   mCherry gene at the 3' end of the *dolP* gene. Gene synthesis was performed by

467   Genscript®. The pet20b+-*wbbL* plasmid for restoring O-antigen synthesis in *E. coli*

468   K-12 was previously described[47]. Single point mutations were generated by using

469   Quickchange II according to manufacturer's instructions. All constructs were

470   confirmed by DNA sequencing. Strains were routinely cultured on LB agar and LB

471   broth. Linker scanning mutagenesis was performed with an Ez-Tn5 kit (Epicentre®)

472   as previously described[48].

473

474   **Analysis of membrane lipid content.** Cell envelopes of *E. coli* were separated by

475   defined sucrose density gradient separation, precisely as described previously

476   following cell disruption by 3 passes of the C3 emulsiflex (Avestin)[49,50]. Samples

477   were generated in biological triplicate from three separate 2 L batches of cells grown

478   to an OD_{600} 0.6-0.8, with the final volumes for washed membranes being 1 ml, which

479   were stored at -80˚C until analysis. Lipids were extracted by the Bligh-Dyer method[51]

480   from purified membranes as described previously[49]. Methanol and chloroform were

481   added to the samples to extract the metabolites using a modified Bligh-Dyer

482   procedure[52] with a final methanol/chloroform/water ratio of 2:2:1.8. The non-polar

layer was extracted and dried under nitrogen before being stored at -80˚C until analysis. Samples were re-dissolved in 200 µl chloroform before being separated by thin layer chromatography on silica gel 60 plates with the mobile phase as chloroform:methanol:water at the following ratio: 65:25:10. Lipids were visualized by staining with phosphomolybdic acid. Analysis of lipid samples by mass spectrometry was completed as described previously [53]. The differences were as follows: lipid extracts were diluted 10x or 20x into starting LC solvent the LC-MS/MS run directly. Normalization was completed by taking the ion intensity of each phospholipid relative to the total ion count.

Biochemical analyses. Cellular fractions were prepared as described previously[54]. Cellular fractions and purified proteins were electrophoresed on 12 or 15% SDS-PAGE gels and stained with Coomassie blue or transferred to a polyvinylidene difluoride (PVDF) membrane for Western immunoblotting as previously described[55]. Loading consistency was confirmed by immuno-blotting with anti-BamB or anti-PqiB antiserum where possible. Protease shaving assays were described previously[56]. Proteins were localized by immunofluorescence as described previously[55]. Analytical ultracentrifugation was performed as described previously[57]. For proteomic analysis of OM protein content, OM fractions purified by defined sucrose gradient centrifugation in biological triplicate and were digested with trypsin using the FASP method[58]. Primary amines in the peptides were then dimethylated using hydrogenated or deuterated formaldehyde and sodium cyanoborohydride. Labelled peptides were mixed, separated into 15 fractions by mixed-mode reverse-phase/anion exchange chromatography, the fractions lyophilized and each analysed with a 90 minute LC-MS/MS run using a Bruker Impact Q-TOF mass spectrometer. Data was searched against forward and randomized *E. coli* sequence databases using MASCOT and filtered at 1% FDR. Quantitation was based on the extracted ion chromatograms of light/heavy peptide pairs. DolP was investigated for binding partners using immunoprecipitation assays as described previously. Briefly, *E. coli* *ΔdolP*, and isogenic strains containing pDolP^{pelB} or plasmid containing a His-Tagged version of BamA were grown in LB media to an OD$_{600}$ of ~0.6 and harvested by centrifugation. Cells were resuspended in PBS with Triton X-100 supplemented with lysozyme and Benzonase nuclease. Cells were lysed and clarified by centrifugation. The lysate was incubated with Ni-NTA agarose (Qiagen) or appropriate antibodies. Precipitated proteins were analysed by Western immunoblotting.

NMR spectroscopy. Experiments were carried out at 298 K on a Varian Inova 800 MHz spectrometer equipped with a triple-resonance cryogenic probe and *z*-axis pulse-field gradients. Isotope labelled DolP (^{15}N ^{13}C) with its N-terminal cysteine replaced was used at a concentration of 1.5 mM in 50 mM sodium phosphate (pH 6), 50 mM NaCl and 0.02% NaN$_3$ in 90% H$_2$O/10% D$_2$O. Spin system and sequential assignments were made from CBCA(CO)NH, HNCACB, HNCA, HN(CO)CA, HNCO, HN(CA)CO, H(C)CH TOCSY and (H)CCH TOCSY experiments[59]. Spectra were processed with NMRPipe[60] and analyzed with SPARKY[61].

Structure calculations. Interproton distance restraints were obtained from ^{15}N- and ^{13}C-edited NOESY-HSQC spectra (τ_{mix}=100 ms). PRE restraints were obtained by adding 10 mM DPC/3.33 mM CHAPS micelles spiked with 1 mM DMPG and 0.185 mM 5-doxyl 1-palmitoyl-2-steroyl-sn-glycero-phosphocholine (Avanti, Polar Lipids, Alabaster, AL, USA) to ^{15}N-labelled DolP (300µM) and by standardizing amide resonance intensities to those induced by spiking instead with unlabelled dipalmitoyl phosphocholine (Avanti Polar Lipids). Backbone dihedral angle restraints (ϕ and ψ) were obtained using TALOS from the backbone chemical shifts[62]. Slowly exchanging amides were deduced from the ^{1}H ^{15}N SOFAST-HSQC[63] spectra of protein dissolved in 99.96% D$_2$O. The structure was calculated iteratively using CANDID/CYANA, with automated NOE cross-peak assignment and torsion angle dynamics implemented[64]. A total of 20 conformers with the lowest CYANA target function were produced that satisfied all measured restraints. Aria1.2 was used to perform the final water minimization[65]. Structures were analysed using PROCHECK-NMR[66] and MOLMOL[67]. Structural statistics are summarized in **Table 2**.

Lipid interactions. Ligand binding to 300 µM ^{15}N- DolP in 50 mM sodium phosphate (pH 6), 50 mM NaCl and 0.02% NaN$_3$ in 90% H$_2$O/10% D$_2$O was monitored by ^{1}H^{15}N-HSQCs at concentrations of 0–40 mM of either DHPG or DHPE (c.m.c., ~7 mM). The DPC-DMPG: DolP complex was calculated by HADDOCK[22,68]. A total of 18 paramagnetic relaxation enhancements restrained the distances between the micelle centre and the respective NH groups to 0-20 Å, with CSPs defining the flexible zone. The top 200 models were ranked according to their experimental energies and statistics derived from the 20 lowest energy conformers were reported **(Table 5)**.

Small angle X-ray scattering. Synchrotron SAXS data of DolP were collected at the EMBL X33 beamline (DESY, Hamburg) using a robotic sample changer. DolP

concentrations between 1-10 mg/ml were run in 50 mM sodium phosphate (pH 6), 50 mM NaCl and 0.02% NaN_3. Data were recorded on a PILATUS 1M pixel detector (DECTRIS, Baden, Switzerland) at a sample-detector distance of 2.7 m and a wavelength of 1.5 Å, covering a range of momentum transfer of 0.012 < s < 0.6 Å^{-1} (s = 4πsin(θ)/γ, where 2θ is the scattering angle) and processed by PRIMUS[69]. The forward scattering I(0) and the radius of gyration (R_g) were calculated using the Guinier approximation[70] **(Figure 2-figure supplement 6)**. The pair-distance distribution function pR, from which the maximum particle dimension (D_{max}) is estimated, was computed using GNOM[71] **(Figure 2-figure supplement 6)**. Low resolution shape analysis of the solute was performed using DAMMIF[72]. Several independent simulated annealing runs were performed and the results were analysed using DAMAVER[73]. Back comparison of the DolP solution structure with the SAXS data was performed using the ensemble optimisation method[74] accounting for flexibility between residues 20-46, 112-118 and 189-195. All programs used for analysis of the SAXS data belong to the ATSAS package[75].

Accession codes. Coordinates and NMR assignments have been deposited with accession codes 7A2D (PDB) and 19760 (BMRB), respectively.

Cell imaging.

Cultures were grown at 37°C to OD_{600} 0.4-0.5. Cells were harvested by centrifugation at 7000 x g for 1 min before being applied to agarose pads, which were prepared with 1.5 % agarose in PBS and set in Gene Frames (Thermo Scientific). Cells were immediately imaged using a Zeiss AxioObserver equipped with a Plan-Apochromat 100x/Oil Ph3 objective and illumination from HXP 120V for phase contrast images. Fluorescence images were captured using the Zeiss filter set 45, with excitation at 560/40 nm and emission recorded with a bandpass filter at 630/75 nm. For localization analysis and generation of demographs, the MicrobeJ plugin for Fiji was used and >500 cells were used as input for analysis[76].

Membrane fluidity assay. Membrane fluidity was measured by use of the membrane fluidity assay kit (Abcam: ab189819) as was described previously except with minor modifications[21]. Specific bacterial strains were grown to stationary phase overnight (~16 hrs) after which cells were harvested by centrifugation, washed with PBS three times and finally labelled with labelling mix (10 µM pyrenedecanoic acid and 0.08% pluronic F-127 in PBS) for 20 minutes in the dark at 25°C with shaking.

586   Cells were washed twice with PBS before fluorescence was recorded with excitation

587   at 350 nm and emission at either 400 nm or 470 nm to detect emission of the

588   monomer or excimer respectively. Unlabelled cells were used as a control to confirm

589   labelling and the *E. coli* BW25113 Δ*waaD* strain was used as a positive control for

590   increased membrane fluidity. Following subtraction of fluorescence from the blanks,

591   averages from triplicate experiments were used to calculate the ratio of excimer to

592   monomer fluorescence. These ratios were then expressed as relative to the parent

593   *E. coli* BW25113 strain.

594

595   **Genetic interaction analysis.** Genetic interaction assay was performed as

596   described in[77]. For each probed strain, a single source plate was generated and

597   transferred to the genetic interaction plate using a pinning robot (Biomatrix 6). On

598   each genetic interaction assay plate, the parental strain, the single deletion A, the

599   single deletion B and the double deletion AB were arrayed, each in 96 copies per

600   plate. Genetic interaction plates were incubated at 37°C for 12 h and imaged under

601   controlled lighting conditions (spImager S&P Robotics) using an 18-megapixel

602   Canon Rebel T3i (Canon). Colony integral opacity as fitness readout was quantified

603   using the image analysis software Iris[78]. Fitness ratios were calculated for all

604   mutants by dividing their fitness values by the respective WT fitness value. The

605   product of single mutant fitness ratios (expected) was compared to the double

606   mutant fitness ratio (observed) across replicates. The probability that the two means

607   (expected and observed) are equal across replicates is obtained by a Student's two-

608   sample *t*-test.

609

610   **Lipid A Palmitoylation assay.** Labelling of LPS, Lipid A purification, TLC analysis

611   and quantification were done exactly as described previously[79]. The positive control

612   was exposed to 25 mM EDTA for 10 min prior to harvest of cells by centrifugation in

613   order to induce PagP mediated palmitoylation of Lipid A[79]. Experiments were

614   completed in triplicate and the data generated was analyzed as described

615   previously.

Figure 1 - DolP is a conserved BON domain protein with a distinct role in OM homeostasis.

A. In *E. coli*, *dolP* is located downstream of *diaA* and encodes a lipoprotein with a signal sequence (orange) and two BON domains (red). The signal sequence is cleaved by LspA, the cysteine at position 19 acylated by Lgt and Lnt and finally the protein is targeted to the OM by the Lol system **(Figure 1-figure supplement 1)**. *E. coli* contains three BON domain proteins. DolP shares a similar domain organization with OsmY, which encodes a periplasmic protein that possesses a signal sequence (green) which is recognised and cleaved by the signal peptidase LepB. Kbp is more divergent from DolP and OsmY, has no predictable signal sequence and is composed of BON and LysM domains **(Figure 1-figure supplement 2)**. **B.** DolP, OsmY and Kbp are widespread among proteobacteria, and cluster into three distinct groups based on the program CLANS[42] with connections shown for a *P* value cut-off of $<10^{-2}$ (**Table 4**). **C.** Growth phenotypes for mutant isolates lacking DolP ($\Delta dolP$), wild-type strain (WT) or the complemented mutant (COMP). Strains were grown on LB agar containing vancomycin (100 μg/ml) or sodium dodecyl sulphate (SDS; 4.8%). **D.** DolP from diverse proteobacterial species expressed in an *E. coli* $\Delta dolP$ strain restores growth in the presence of vancomycin as assessed by a serial dilution plate growth assay. Plasmids expressing OsmY do not complement the defect.

Figure 2 - Structure of DolP. A. Solution structure and topology of DolP, with α helices, β strands and termini labelled. **B.** Backbone model of the 20 lowest-energy solution structures of DolP. The core folded domain is highlighted in red whilst the flexible N-terminal is shown in grey. The dynamic nature of the linker was demonstrated from S2 order parameter analysis calculated from chemical shift assignments using TALOS+. **C.** Small Angle X-ray Scattering curve of DolP with corresponding best fit of the solution structure of DolP. Best fit calculated based on the core DolP solution structure with flexibility accommodated in residues 20-46, 112-118 and 189-195. The corresponding *ab initio* bead model is shown calculated using Dammif[72] based solely on the scattering data. **D.** Western blots of total protein extracts show plasmid-mediated expression of DolP in *E. coli* $\Delta dolP$ after site-directed mutation of conserved residues. The empty vector (EV) control is labelled and WT represents wild type DolP. The presence of the OM lipoprotein BamB was used as a control. Colony growth assays by serial dilution of mutants on 4.8 % SDS reveal which residues are critical for the maintenance of the OM barrier function. **E.** Structure of DolP showing position of transposon-mediated insertions. Western blots of total protein extracts show plasmid-mediated expression of mutant versions of DolP in *E. coli* $\Delta dolP$. The empty vector (EV) control is labelled and WT represents wild type DolP. Colony growth assays by serial dilution of mutants on 4.8 % SDS reveal which insertions abolish DolP function. Blue labels represent position of non-functional insertions. Orange labels represent position of tolerated insertions. The presence of the OM lipoprotein BamB was used as a control.

Figure 3 - DolP BON2:α1 binds phospholipid. A. DolP ribbon structure highlighting residues exhibiting substantial CSPs ($\Delta\delta_{ave}$) upon DHPG micelle interaction. The histogram shows the normalised perturbations induced in each residue's amide signal when DHPG (40mM) was added to DolP (300 μM). Examples of significant CSPs are shown. **B.** Histogram showing intensity reductions of H_N signals of DolP induced by adding 5-doxyl PC and DMPG into DPC/CHAPs micelles and the corresponding structure of a representative DolP-micelle complex calculated

668 using CSPs and doxyl restraints using the program HADDOCK. Only the BON2:α1
669 helix is observed making contact with the micelle surface. No corresponding
670 interaction of the BON1:α1 helix is observed. Zoom panels show burial of BON2:α1
671 into the micelle. The side chains of DolP residues that intercalate between the acyl
672 chains (G120, S123, W127, T130 and S134) are coloured red. The side chains of
673 residues that buttress the interface (E121, N124, T126, I128, K131, R133 and Q135)
674 are coloured yellow. DolP is shown in blue and the phospholipid micelle is shown in
675 tan.
676
677 **Figure 4 - DolP specifically recognizes anionic phospholipid via BON2:α1**
678 **A.** Histograms showing the normalized CSP values observed in ^{15}N labelled DolP
679 (300 μM) amide signals in the presence of 20 mM 1,2,-dihexanoyl-sn-glycero-3-
680 phosphethanolamine, 20 mM 1,2-dihexanoyl-sn-glycero-3-phospho-(1'-rac-glycerol)
681 and 5 mM cardiolipin. **B.** Mutagenesis of the BON2:α1 helix residues identified by
682 CSPs. The positions of W127 and L137 are indicated as sticks. Western blots of total
683 protein extracts show plasmid-mediated expression of DolP in *E. coli* $\Delta dolP$ after
684 site-directed mutation of amino acid residues. The empty vector (EV) control is
685 labelled and WT represents wild type DolP. Colony growth assays of *E. coli* $\Delta dolP$
686 complemented with DolP mutants reveal which residues are critical for the
687 maintenance of OM barrier function. The presence of the protein PqiB was used as a
688 control. **C.** Histograms showing the normalized CSP values observed in ^{15}N labelled
689 DolP^{WT} or DolP^{W127E} mutant (300 μM) amide signals in the presence of 40 mM 1,2-
690 dihexanoyl-sn-glycero-3-phospho-(1'-rac-glycerol).
691
692 **Figure 5 - Phospholipid binding is required for DolP recruitment to division**
693 **sites**
694 **A.** Fluorescence microscopy of $\Delta dolP$ cells expressing either DolP^{WT}::mCherry or
695 DolP^{W127E}::mCherry from the pET17b plasmid after growth to mid-exponential phase
696 (OD$_{600}$ ~0.4-0.8). Scale bars represent 2 μM and both phase contrast and the
697 mCherry channel are shown in greyscale and red respectively. White arrows
698 highlight division site localization of DolP^{WT}-mCherry. Demographic representations
699 of the DolP^{WT}-mCherry or DolP^{W127E}-mCherry fluorescence intensities measure
700 along the medial axis of the cells. Images of >500 cells were analyzed using the
701 MicrobeJ software and sorted according to length where the y-axis represents
702 relative cellular position with 0 being mid-cell and 3 or -3 being the cell poles[76]. **B.**
703 Thin layer chromatography of phospholipids extracted from either *E. coli* BW25113
704 (WT), $\Delta rcsF\Delta lpp$, $\Delta rcsF\Delta lpp\Delta pgsA$ (referred to as $\Delta pgsA$) or $\Delta clsA\Delta clsB\Delta clsC$
705 (referred to as Δcls*ABC*) strains. The *rcsF* and *lpp* genes must be removed in order
706 to prevent toxic build-up of Lpp on the IM in the *pgsA* mutant. Phospholipids were
707 separated using chloroform:methanol:acetic acid (65:25:10) as the mobile phase
708 before staining with phophomolybdic acid and charring. **C.** Fluorescence microscopy
709 of $\Delta pgsA$ or Δcls*ABC* cells expressing DolP^{WT}mCherry from the pET17b plasmid
710 after growth to mid-exponential phase (OD$_{600}$ ~0.4-0.8). White arrows highlight DolP-
711 mCherry mislocalization.
712

Figure supplement legends

714

715   **Figure 1-figure supplement 1. DolP is an OM lipoprotein**. **A.** OM fractions of *E.*
716   *coli* BW25113, an isogenic Δ*dolP* mutant and the complemented mutant were
717   analyzed by SDS-PAGE and Western immunoblotting with antibodies to DolP and
718   the known OM lipoproteins BamC and BamE. DolP is not detected in the mutant but
719   like BamC and BamE is found with the membrane fraction. **B.** Western
720   immunoblotting of OM fractions from *E. coli* Δ*dolP* complemented with a plasmid
721   (pDolP-C19A) encoding DolP with a point mutation at position C19. **C.** *E. coli* cells
722   treated with protease in the presence (+) or absence (-) of polymyxin B, which
723   permeablizes the OM, allowing the protease access to the periplasm. Antibodies to
724   the cytoplasmic RNA polymerase (RNAP) and the periplasmic chaperone SurA were
725   used as controls. **D.** Immunofluorescence photomicrographs of *E. coli* BW25113, an
726   isogenic Δ*dolP* mutant and the complemented mutant. Cells were probed with anti-
727   DolP before and after permeabilization. Anti-SurA was used as a control.

728

729   **Figure 1-figure supplement 2. BON domain (Pfam: PF04972) containing**
730   **proteins**. The Pfam database was interrogated for the presence of proteins
731   containing BON domains. BON domains are widely distributed in bacteria and eight
732   major architectures are noted **(Table 1)**. The predominant architecture is that
733   observed for DolP and OsmY where the protein possesses a signal sequence and
734   one or more BON domains. The second major architecture is that observed for Kbp,
735   where proteins possess one or more BON domains and a LysM domain. The other
736   major architectures include associations with Secretin (Pfam: PF00263), CBS (Pfam:
737   PF00571), OmpA (Pfam: PF00691), MS_channel (Pfam: PF00924), FHA (Pfam:
738   PF00498) or cytidylate kinase (Pfam: PF13189) domains. Due to their functions,
739   many of these domains would place their associated BON domains in proximity to
740   cell membranes.

741

742   **Figure 1-figure supplement 3. DolP has a distinct function from OsmY and**
743   **Kbp**. The precise functions of Kbp and OsmY are unknown, though both are induced
744   during adaptation to hyperosmolarity[29,80-83] **A.** Investigation of *osmY* and *kbp* null
745   mutants of *E. coli* revealed neither was sensitive to vancomycin or SDS. Growth
746   phenotypes for mutant isolates lacking BON domain proteins, wild-type strains (WT)
747   or complemented mutants (COMP). Strains were grown on LB agar containing
748   vancomycin (100 μg/ml) or sodium dodecyl sulphate (SDS; 4.8%). **B.** A plasmid
749   encoding a DolP-OsmY chimeric protein composed of the lipoprotein targeting
750   sequence of DolP and the BON domains of OsmY failed to complement the OM
751   defect associated with loss of *dolP*. **C.** *E. coli* BW25113 Δ*dolP* is not more
752   susceptible to osmotic stress induced by NaCl than the parent strain as assessed by
753   a serial dilution plate assay. Interestingly, our investigations did not reveal a role for
754   either *kbp* or *osmY* in survival of osmotic stress as the *E. coli* BW25113 parent strain
755   and isogenic *osmY::aph* and *kbp::aph* mutants survived equally well.

756

757   **Figure 1-figure supplement 4. Phenotypes of *E. coli* BW25113 Δ*dolP***. **A.** Mutants
758   lacking *dolP* are sensitive to the anionic detergents cholate and deoxycholate **B.**
759   Mutants lacking *dolP* have growth rates that are indistinguishable from wild-type *E.*
760   *coli*. **C.** Scanning electron microscopy reveals parental and *E. coli* Δ*dolP* cells have
761   no discernible differences in cellular morphology.

762

763   **Figure 1-figure supplement 5. Localization of DolP to the OM is required for**
764   **function**. The signal sequence and domain architecture of DolP are shown. The

765 sequence changes to pET17b-*dolP^WT* to create the construct targeting DolP to the
766 IM (pET17b-*dolP^IM*) are shown in red. The signal sequence of *dolP* was also
767 swapped for that of *pelB* in order to create the construct pET17b-*dolP^pelB* in order to
768 target DolP to the periplasmic space with no modification. Fluorescence microscopy
769 of Δ*dolP* cells expressing either DolP^WT-mCherry or DolP^IM-mCherry or DolP^pelB-
770 mCherry from the pET17b plasmid after growth to mid-exponential phase (OD_{600}
771 ~0.4-0.8). Scale bars represent 2 μM and both phase contrast and the mCherry
772 channel are shown in greyscale and red respectively. The capacity of DolP^WT,
773 DolP^IM, DolP^WT-mCherry or DolP^IM-mCherry to complement the Δ*dolP* mutant
774 sensitivity phenotype was screened by dilution assay on 4.8 % SDS. The expression
775 of each construct was checked by Western blotting of total protein extracts with anti-
776 DolP antiserum.
777
778 **Figure 2-figure supplement 1. DolP is monomeric**. **A.** DolP, lacking the site of
779 acylation, was purified and subject to analytical ultracentrifugation. DolP
780 demonstrated a uniform sedimentation velocity consistent with a monomeric species.
781 **B.** Column chromatography of purified DolP revealed that it had an elution profile
782 consistent with a single monomeric species.
783
784 **Figure 2-figure supplement 2. Structural analysis of the DolP BON domains**. **A.**
785 The ensemble of the 20 lowest energy structures superimposed to DolP BON1 (N47-
786 I111) and BON2 (G120-T185) domain backbones showing how well the domains
787 superimpose as well as the respective degrees of freedom available to each domain.
788 **B.** Dalilite superposition of DolP BON domains 1 (Red; residues 46-114) and 2 (Blue;
789 residues 117-189). The BON domains are similar except for the double turn
790 extension of the BON2:α1 helix and the presence of the α1' helix present in BON1
791 that is absent in BON2. The pairwise RMSD for backbone heavy atoms is 1.8 Å and
792 dalilite Z-score is 8.4. **C.** Superposition of DolP BON2 (Blue) on to the BON
793 subdomain of Rv0899 (OmpATb) (Green; accession code – 2KSM; residues 136-
794 196). For BON2 the pairwise RMSD for backbone heavy atoms was 2.7 Å and the
795 dalilite Z-score was 4.9. Similarly, for BON1 the pairwise RMSD was 2.6 Å and the
796 dalilite Z-score was 5.3**.**
797
798 **Figure 2-figure supplement 3. Alignment of DolP sequences from diverse**
799 **proteobacterial species**. **A.** The amino acid sequences of the experimentally
800 derived BON domains of DolP and OmpATb are aligned with the predicted amino
801 acid sequences of the BON domains from Kbp and OsmY. The position of the
802 experimentally derived secondary structure for DolP BON1 and BON2 and OmpATb
803 are depicted below the sequence alignment. **B.** Alignments of the amino acid
804 sequences of DolP and OsmY from various Gram-negative bacteria. The positions of
805 the experimentally-derived secondary structural elements of *E. coli* DolP are
806 depicted below the sequence alignment. The signal sequence is depicted by the red
807 box. The Lipobox associated with recognition by LspA and acylation is highlighted in
808 purple. The conserved glycine residues are highlighted in blue and the tyrosine
809 residue associated with interdomain interactions is highlighted in green. Residues
810 showing CSPs are highlighted in pink.
811
812 **Figure 2-figure supplement 4. Additional SAXS analysis of DolP. A.** Zoom in of
813 the low s region of the small angle X-ray scattering curve of DolP shown in Figure 2
814 highlighting the closeness of fit to the DolP solution structure. **B.** Residuals plot
815 between the DolP solution structure and the small angle X-ray scattering curve
816 highlighting the closeness of fit.

817

Figure 2-figure supplement 5. Representation of DolP interdomain interactions highlighting the location of interdomain NOEs identified. 38 interdomain NOEs were identified via Cyana **(Table 3)**. Due to the ambiguity between chemically equivalent hydrogens within the same group, multiple NOEs are displayed to all equivalent hydrogens resulting in 83 NOEs being displayed.

Figure 2-figure supplement 6. SAXS processing analysis. A. The linear region of the Guinier plot measured from the raw SAXS data for DolP. Values for Rg and I(0) are shown calculated using AutoRG in program Primus. **B.** Pair-wise distance distribution P(r), calculated from the scattering curve of DolP, calculated using gnom arbitrary units (a.u.).

Figure 3-figure supplement 1. *dolP* has genetic interactions with *bamB* and *bamE* but no detectable physical interaction. A. *dolP* genetically interacts with the genes encoding the non-essential BAM complex accessory lipoproteins. Strains were arrayed on LB Lennox agar plates using a Biomatrix 6 replicator. Genetic interaction plates were incubated for 12h at 37°C and imaged. An example of a 384-well plate is shown above the graph. Each plate contained a total of 384 colonies consistent of 96 wildtype, single and double mutant clones. Fitness was measured by quantifying colony size and integral opacity, which represents colony density, using the image analysis software Iris[78]. Bar plots show the averaged values 96 technical replicates. The error bars represent the 95% confidence interval. **B.** Phase contrast microscopy of WT, Δ*dolP*, Δ*bamB*, Δ*bamC,* Δ*bamE,* Δ*bamB*Δ*dolP*, Δ*bamC*Δ*dolP* and Δ*bamE*Δ*dolP* cells after growth to mid-exponential phase (OD$_{600}$ ~0.4-0.8). Scale bars represent 2 μM. Phase light cells can be observed for the Δ*bamB*Δ*dolP* and Δ*bamE*Δ*dolP* cells. **C.** DolP immunoprecipitation. Whole cell triton X-100 solubilised lysates of *E. coli* BW25113 pDolP^{pelB}, pBamA-His and Δ*dolP*, were purified by Ni-NTA affinity chromatography then detected by western blot using anti-DolP and BamA-E antibodies. **D.** Purified OM samples from *E. coli* BW25113 parent (WT) or Δ*dolP* cells were separated by SDS-PAGE, with (d) and without (n) boiling before being visualized by staining with coomassie.

Figure 3-figure supplement 2. Loss of DolP affects membrane fluidity, but does not affect membrane lipid profiles. **A.** SDS-PAGE gel showing separation of LPS preparations from *E. coli* BW25113 and *E. coli* BW25113 harboring pET20b-*wbbL* which restores O-antigen expression on the bacterial cell surface. **B.** Analysis of phospholipid profiles from purified Δ*dolP* cell envelopes. Phospholipids were extracted by the Bligh-Dyer method from *E. coli* IM or OM samples purified by sucrose density gradient centrifugation. Phospholipids were visualized by staining with phosphomolybdic acid and charring after being separated by thin-layer chromatography with the following mobile phase: Chloroform:methanol:acetic acid (65:25:10). Phospholipid profiles were also analysed by LC/MS-MS following separation on the Luna C8(2) column under a THF/MeOH/H$_2$O gradient. Phospholipid compositions are shown as sum for each of the four major classes observed: lyso-phophatidylethanolamines (LysoPE), phosphatidylethanolamines (PE), phosphatidylglycerols (PG) and cardiolipins (CL). Each data set is from three biological replicates generated from three separately purified membranes. Error bars represent ±S.D. **C.** PagP-mediated Lipid A palmitoylation assay. PagP transfers an acyl chain from surface exposed phospholipid to hexa-acylated Lipid A to form hepta-acylated Lipid A. [32P]-labelled Lipid A was purified from cells grown to mid-exponential phase in LB broth with aeration. Equal amounts of radioactive material

869 (cpm/lane) was loaded on each spot and separated by thin-layer chromatography
870 before quantification. As a positive control, cells were exposed to 25 mM EDTA for
871 10 min prior to Lipid A extraction in order to chelate Mg^{2+} ions and destabilize the
872 LPS layer, leading to high levels of Lipid A palmitoylation. Hepta-acylated and hexa-
873 acylated lipid A was quantified and hepta-acylated Lipid A represented as a
874 percentage of total. Triplicate experiments were utilized to calculate averages and
875 standard deviations with students t-tests used to assess significance. Student's *t*-
876 tests: NS* *P* > 0.1 compared with Parent EV. **D.** *E. coli* BW25113 cells were grown
877 overnight in LB (~16hrs) before being harvested by centrifugation and washed three
878 times in PBS. Membrane fluidity was measured for each strain in triplicate and error
879 bars represent standard deviation. Membrane fluidity is expressed as relative to *E.*
880 *coli* BW25113 parent cells (WT).

882 **Figure 3-figure supplement 3. DolP phosphatidylglycerol binding HSQC**
883 **spectra. A**. $^1H,^{15}N$ HSQC spectra of ^{15}N-DolP (300 μM) in the presence (red) and
884 absence (black) of 40 mM 1,2-dihexanoyl-sn-glycero-3-phospho-(1'-rac-glycerol)
885 (DHPG) highlighting the large chemical shift perturbations observed on DHPG
886 binding. **B.** Histograms showing the normalised CSP values observed in ^{15}N labelled
887 DolP (300 μM) amide signals in the presence of 5 mM cardiolipin, 20 mM 1,2,-
888 dihexanoyl-sn-glycero-3-phosphethanolamine and 20 and 40 mM 1,2-dihexanoyl-sn-
889 glycero-3-phospho-(1'-rac-glycerol).

891 **Figure 3-figure supplement 4. Kd estimation from HSQC titration data.** Kd
892 estimation was performed using the sum of the average chemical shift distance
893 plotted against ligand concentration and fit using a standard ligand binding curve.
894 Representative fits for G120, W127 and T138 are shown with corresponding
895 estimations for Bmax, the maximum Δδppm, and Kd highlighted.

897 **Figure 4-figure supplement 1. Electrostatic analysis of DolP**. **A.** Electrostatic
898 surface map of DolP BON domains 1 and 2 calculated using DelPhi[84] at a pH of 6
899 and 0.05M ionic strength (which approximates the experimental conditions). The -
900 3kT/e surface is shown in red and the +3kT/e surface is shown in blue. A formal
901 charge library was used, with a dielectric of 2 assigned to the protein interior and a
902 dielectric of 80 assigned to the exterior. Cartoon representations of the BON
903 structures are shown to the right of each surface to more clearly highlight the
904 orientations of the protein. The BON1:α1 and BON2:α1 helices show clear
905 differences, with BON1:α1 being predominantly neutral with an electronegative patch
906 towards its N-terminus, whilst BON2:α2 shows no electronegatively at all, but rather
907 has a large electropositive patch towards the center of this helix presumably
908 explaining its specificity for the electropositive surface of phosphatidylglycerol. **B.**
909 Hydrophobic surface map of DolP BON domains 1 and 2, hydrophobic residues (A,
910 G, V, I, L, F, M) are shown in cyan, W127 (Red) is shown exposed on the surface of
911 the BON2:α1 helix. Cartoon representations of the BON structures are shown to the
912 right of each surface to more clearly highlight the orientations of the protein.

914 **Figure 4-figure supplement 2. Analysis of DolP mutants**. **A.** *E. coli* BW25113
915 $\Delta dolP$ mutants were complemented with plasmids expressing a wild-type copy of
916 DolP or a mutant version. Each strain was serially diluted and plated on LB-agar
917 containing either vancomycin (100 μg/ml) or SDS (4.8% wt/vol) and growth was
918 observed after overnight incubation. The W127E and L137E mutants failed to grow.
919 **B.** Western immunoblotting of whole cell lysates derived from overnight cultures of

920 mutants highlighted in the top panel. Blots were probed with antibodies to the outer
921 membrane lipoprotein BamB and to DolP.
922
923 Figure 1-figure supplement 1-source data 1
924
925 Figure 1-figure supplement 4-source data 1
926
927 Figure 1-figure supplement 5-source data 1
928
929 Figure 2-source data 1
930
931 Figure 3-source data 1
932
933 Figure 3-source data 2
934
935 Figure 3-figure supplement 1-source data 1
936
937 Figure 3-figure supplement 2-source data 1
938
939 Figure 3-figure supplement 2-source data 2
940
941 Figure 3-figure supplement 2-source data 3
942
943 Figure 3-figure supplement 2-source data 4
944
945 Figure 4-source data 1
946
947 Figure 5-source data 1
948
949

Table 1. Taxonomic distribution of BON family domain architectures.

Cluster number[a]	UniRef100[b]	Total number of proteins[c]	Major domain architecture in cluster[d]	Alpha	Beta	Gamma	Delta	Epsilon	Zeta	Acidobacteria	Actinobacteria	Bacteroidetes	Chlamydiae	Chlorobi	Chloroflexi	Cyanobacteria	Deinococcus-Thermus	Fibrobacteres	Firmicutes	Gemmatimonadetes	Nitrospirae	Planctomycetes	Spirochaetes	Synergistetes	Thermobaculum	Thermodesulfobacteria	Thermotogae	Verrucomicrobia
1	1280	2723	OsmY-like and 1 x BON	41 (89)[e,f]	176 (533)	1484 (1830)	33 (56)	12 (12)	1 (1)	6 (12)	2 (3)	5 (5)	3 (11)		3 (4)	43 (65)	1 (1)		13 (13)	1 (2)	1 (1)	14 (30)	9 (9)		1 (1)	1 (1)		7 (19)
2	833	2395	DolP-like	97 (103)	330 (335)	1892 (1919)	15 (17)	2 (2)											1 (1)			1 (2)				1 (1)		
3	579	690	3 x BON + 1 x BON	95 (187)	108 (255)	35 (36)	18 (28)			7 (23)	14 (25)	14 (30)	2 (2)		3 (21)	6 (10)	5 (7)	1 (1)	32 (32)	1 (2)		12 (27)				1 (1)		
4	476	537	BON + secretin	207 (276)	77 (80)	70 (117)	32 (34)			4 (4)	1 (1)			3 (3)					10 (11)		1 (1)	7 (7)		1 (1)				
5	409	1570	Kbp-like	66 (66)	131 (132)	1323 (1328)	1 (1)	1 (1)				31 (31)	4 (4)			5 (5)			1 (1)					1 (1)				
6	282	300	CBS + CBS + BON	82 (136)	17 (29)	4 (4)					53 (127)	4 (4)																
7	220	318	BON + BON + OmpA	157 (161)	55 (57)	9 (11)					62 (64)	1 (1)				19 (23)					1 (1)							
8	70	75	BON + Mschannel	31 (32)	1 (1)	24 (25)	2 (3)										1 (1)					8 (13)					
9	52	52	1 x BON		1 (1)											42 (51)												
10	43	80	1 x BON and 1 x DUF2204		1 (1)	1 (1)					77 (77)																	1 (1)
11	33	87	1 - 2 X Forkhead + BON	2 (2)	4 (4)							2 (2)	78 (79)														
12	30	33	1 x BON		26 (27)		3 (3)				1 (1)				1 (1)							1 (1)						
smaller cluster/unclustered:																											
	83	109		22 (29)	19 (19)	25 (25)					9 (9)				1 (1)							4 (12)		2 (2)			1 (1)	

[a]The main twelve clusters were analyzed, all proteins falling into smaller clusters were summarized into the single category "smaller cluster".

[b,c,d,e]Shown are the number of UniRef100 used in the clustering approach[b], the corresponding number of proteins derived from the HMMER search[c], the observed major domain architecture[d] and the number of unique protein sequences (in brackets)[e] as well as the number of unique organisms mapped to the bacterial (Sub)Phyla[f].

955 **Table 2.** Structural statistics of the ensemble of 20 DolP solution structures

	DolP
Completeness of resonance assignments[b]	
Aromatic completeness	74.14%
Backbone completeness	98.42%
Sidechain completeness	84.84%
Unambiguous CH2 completeness	100%
Unambiguous CH3 completeness	100%
Unambiguous sidechain NH2 completeness	100%
Conformationally restricting restraints[c]	
Distance restraints	
Total NOEs	2930 (2762)
Intra residue (i = j)	408 (374)
Sequential (| i – j | = 1)	869 (783)
Medium range (1 < | i - j | < 5)	773 (741)
Long range (| i – j | $\geq$ 5)	880 (866)
Interdomain	38
Dihedral angle restraints	258
Hydrogen bond restraints	128
No. of restraints per residue	16.6 (20.9)
No. of long range restraints per residue	5.0 (6.5)
Residual restraint violations[c]	
Average No. of distance violations per structure	
0.2 Å-0.5 Å	3.55
> 0.5 Å	0
Average No. of dihedral angle violations per structure	
> 5o	0 (max 4.8)
Model Quality[c]	
Global (residues 46-190)	
Rmsd backbone atoms (Å)[d]	0.5
Rmsd heavy atoms (Å)[d]	0.9
Domain 1 (Residues 46-112)	
Rmsd backbone atoms (Å)	0.3
Rmsd heavy atoms (Å)	0.7
Domain 2 (Residues 118-190)	
Rmsd backbone atoms (Å)	0.3
Rmsd heavy atoms (Å)	0.8
Rmsd bond lengths (Å)	0.005
Rmsd bond angles (o)	0.6
MolProbity Ramachandran statistics[c.d]	
Most favoured regions (%)	95.1
Allowed regions (%)	4.3
Disallowed regions (%)	0.7
Global quality scores (raw/Z score)[c]	
Verify 3D	0.38/-1.28
Prosall	0.52/-0.54

30

Procheck (phi-psi)[d]	-0.28/-0.79
Procheck (all)[d]	-0.75/-4.44
Molprobity clash score	47.99/-6.71
Model Contents	
Ordered residue ranges[d]	45-193
Total number of residues	178
BMRB accession number	19760
PDB ID code	7A2D

956
957 [a]Structural statistics computed for the ensemble of 20 deposited structures
958 [b]Computed using AVS software[85] from the expected number of resonances, excluding highly
959 exchangeable protons (N-terminal, Lys, amino and Arg guanido groups, hydroxyls of Ser,
960 Thr, and Tyr), carboxyls of Asp and Glu, non-protonated aromatic carbons, and the C-
961 terminal His$_6$ tag.
962 [c]Calculated using PSVS version 1.5[86]. Average distance violations were calculated using the
963 sum over r^{-6}.
964 [d]Based on ordered residue ranges [S(φ) + S(ψ) > 1.8].
965 Values in (brackets) refer to the core structured region.
966

967 **Table 3.** Interdomain NOE restraints identified by Cyana during automated NOE
968 assignment and structure calculation.
969

970

Proton Pair	Intensity	Distance (Å)
TYR 75 HD1 - THR 188 HA	Weak	5.5
TYR 75 HE1 - GLY 160 HA2	Weak	5.4
TYR 108 HE1 - ALA 186 HA	Weak	5.5
TYR 108 HE2 - ALA 186 HA	Weak	5.5
TYR 108 HE1 - ALA 186 HB	Weak	5.1
TYR 75 HD1 - ALA 186 HB	Weak	5.2
TYR 75 HE1 - LEU 161 HA	Weak	5.2
TYR 75 HE1 - LEU 161 HB3	Weak	5.4
TYR 75 HE1 - LEU 161 HG	Weak	5.5
TYR 75 HE1 - LEU 161 HD1	Weak	4.9
TYR 75 HE1 - LEU 161 HD2	Weak	4.9
THR 73 HG2 - ALA 186 HB	Weak	5.5
LYS 78 HD2 - PHE 187 H	Weak	5.5
LYS 78 HD3 - PHE 187 H	Weak	5.5
TYR 75 HD1 - HET 159 HA	Weak	5.5
TYR 108 HD1 - ALA 186 HB	Weak	5.5
GLN 76 HE22 - LEU 161 HB2	Weak	5.2
GLN 76 HE22 - LEU 161 HG	Weak	5.1
GLN 76 HE22 - LEU 161 HD1	Weak	4.5
GLN 76 HE22 - LEU 161 HD2	Weak	4.5
TYR 75 HD1 - THR 188 HG2	Weak	4.2
TYR 75 HE1 - LEU 161 H	Weak	4.3
TYR 75 HE1 - VAL 162 H	Weak	5.5
TYR 75 HE1 - LEU 161 HB2	Weak	4.1
TYR 75 HE1 - THR 188 HG2	Weak	4.1
TYR 75 HE1 - THR 188 H	Weak	5.5
TYR 75 HE1 - GLY 160 H	Weak	4.8
TYR 75 HD1 - GLY 160 H	Weak	4.7
THR 73 HG2 - HET 159 HG	Weak	4.4
TYR 75 HE1 - LEU 161 HD	Weak	4.0
TYR 75 HE2 - LEU 161 HD	Weak	5.1
GLN 76 HE21 - LEU 161 HD	Medium	3.7
GLN 76 HE22 - LEU 161 HD	Medium	3.7
LYS 78 HG - PHE 187 H	Weak	4.9
LYS 78 HD - ALA 186 HB	Weak	5.1
LYS 78 HD - PHE 187 H	Weak	4.7
LYS 78 HE - PHE 187 H	Weak	5.3
ARG 112 HA - ARG 182 HB	Weak	5.3

971 **Table 4.** Accession numbers for the sequences used for CLANS clustering shown in
972 Figure 1

Organism	OsmY	DolP	Kbp
Escherichia coli K12	P0AFH8	P64596	P0ADE6
Klebsiella pneumoniae MGH 78578	A6THZ1	A6TEG9	A6T985
Enterobacter cloacae ENHKU01	J7G7C8	J7GHD1	J7GFT3
Salmonella enterica Typhimurium	Q7CP68	Q7CPQ6	Q8ZML9
Erwinia billingiae Eb661	D8MMS8	D8MME2	D8MNV6
Serratia proteamaculans 568	A8G9G9	A8GJZ3	A8GFP7
Cronobacter sakazakii ATCC BAA-894	A7MGB6	A7MIQ1	A7MEA9
Pantoea sp. Sc1	H8DPK0	H8DQ90	H8DIH9
Hafnia alvei ATCC 51873	G9Y3J7	G9Y4J4	G9YAM4
Citrobacter rodentium ICC168	D2TRY4	D2TQ24	D2TM58
Shigella flexneri 1235-66	I6F1Q5	I6GLP1	I6HD15
Yersinia enterocolitica 8081	A1JJ93	A1JR75	
Yersinia pestis KIM10+	Q7CG58	Q8D1R6	
Dickeya dadantii 3937	E0SJX0	E0SHF6	

973
974

975 **Table 5.** HADDOCK docking statistics for ensemble 20 lowest energy DolP-DPC
976 micelle solution structures calculated

Experimental parameters[a]	
Ambiguous distance restraints	19 including NH of I20, G120-T130, V132-Q135, T138, S139 and NHε of W127
Number of flexible residues[b]	50 (I20-V45 (flexible linker as ascertained by NMR), A74, G120-I128, K131-R133, Q135-L137, V142-S145, I173,S178-V180)
Atomic pairwise RMSD (Å)	
All backbone	
Flexible interface backbone	
Intermolecular energies (kcal.mol^{-1})	
E_{vdw}	-100.81 ± 7.74
E_{elec}	-231.67 ± 64.14
$E_{restraints}$	22.30 ± 4.29
Buried surface area (Å^2)	2186.78 ± 133.277

977 [a]deduced from intensity reductions observed in presence of 5-doxl derivative
978 [b]according to their surface accessibility and the chemical shift perturbation in presence of
979 DPC/CHAPS
980
981

References

982 **References**

983

984 1   May, K. L. & Grabowicz, M. The bacterial outer membrane is an evolving antibiotic
985   barrier. *Proceedings of the National Academy of Sciences of the United States of*
986   *America* **115**, 8852-8854 (2018).
987 2   Konovalova, A., Kahne, D. E. & Silhavy, T. J. Outer Membrane Biogenesis. *Annual*
988   *review of microbiology* **71**, 539-556 (2017).
989 3   Leyton, D. L., Rossiter, A. E. & Henderson, I. R. From self sufficiency to dependence:
990   mechanisms and factors important for autotransporter biogenesis. *Nat Rev*
991   *Microbiol* **10**, 213-225 (2012).
992 4   Babu, M. M. *et al.* A database of bacterial lipoproteins (DOLOP) with functional
993   assignments to predicted lipoproteins. *J Bacteriol* **188**, 2761-2773 (2006).
994 5   Egan, A. J. F. Bacterial outer membrane constriction. *Mol Microbiol* **107**, 676-687
995   (2018).
996 6   Ekiert, D. C. *et al.* Architectures of Lipid Transport Systems for the Bacterial Outer
997   Membrane. *Cell* **169**, 273-285.e217 (2017).
998 7   Stubenrauch, C. J. & Lithgow, T. The TAM: A Translocation and Assembly Module of
999   the beta-Barrel Assembly Machinery in Bacterial Outer Membranes. *EcoSal Plus* **8**
1000   (2019).
1001 8   Gray, A. N. *et al.* Coordination of peptidoglycan synthesis and outer membrane
1002   constriction during Escherichia coli cell division. *eLife* **4** (2015).
1003 9   Goodall, E. C. A. *et al.* The Essential Genome of Escherichia coli K-12. *mBio* **9** (2018).
1004 10   Morris, F. C. *et al.* YraP Contributes to Cell Envelope Integrity and Virulence of
1005   Salmonella enterica Serovar Typhimurium. *Infect Immun* **86** (2018).
1006 11   Bos, M. P., Grijpstra, J., Tommassen-van Boxtel, R. & Tommassen, J. Involvement of
1007   Neisseria meningitidis lipoprotein GNA2091 in the assembly of a subset of outer
1008   membrane proteins. *J Biol Chem* **289**, 15602-15610 (2014).
1009 12   Tsang, M. J., Yakhnina, A. A. & Bernhardt, T. G. NlpD links cell wall remodeling and
1010   outer membrane invagination during cytokinesis in Escherichia coli. *PLoS Genet* **13**,
1011   e1006888 (2017).
1012 13   Carlson, M. L. *et al.* Profiling the Escherichia coli membrane protein interactome
1013   captured in Peptidisc libraries. *eLife* **8** (2019).
1014 14   Babu, M. *et al.* Global landscape of cell envelope protein complexes in Escherichia
1015   coli. *Nat Biotechnol* **36**, 103-112 (2018).
1016 15   Typas, A. *et al.* Regulation of peptidoglycan synthesis by outer-membrane proteins.
1017   *Cell* **143**, 1097-1109 (2010).
1018 16   Ishida, T. *et al.* DiaA, a novel DnaA-binding protein, ensures the timely initiation of
1019   *Escherichia coli* chromosome replication. *J Biol Chem* **279**, 45546-45555 (2004).
1020 17   Dartigalongue, C., Missiakas, D. & Raina, S. Characterization of the Escherichia coli
1021   sigma E regulon. *J Biol Chem* **276**, 20866-20875 (2001).
1022 18   Yeats, C. & Bateman, A. The BON domain: a putative membrane-binding domain.
1023   *Trends Biochem Sci* **28**, 352-355 (2003).
1024 19   Cowles, C. E., Li, Y., Semmelhack, M. F., Cristea, I. M. & Silhavy, T. J. The free and
1025   bound forms of Lpp occupy distinct subcellular locations in Escherichia coli. *Mol*
1026   *Microbiol* **79**, 1168-1181 (2011).

1027	20	Webb, C. T. *et al.* Dynamic association of BAM complex modules includes surface exposure of the lipoprotein BamC. *Journal of molecular biology* **422**, 545-555 (2012).
1029	21	Storek, K. M. *et al.* The Escherichia coli β-Barrel Assembly Machinery Is Sensitized to Perturbations under High Membrane Fluidity. *Journal of bacteriology* **201** (2019).
1031	22	Dominguez, C., Boelens, R. & Bonvin, A. M. HADDOCK: a protein-protein docking approach based on biochemical or biophysical information. *J Am Chem Soc* **125**, 1731-1737 (2003).
1034	23	Oliver, P. M. *et al.* Localization of anionic phospholipids in Escherichia coli cells. *J Bacteriol* **196**, 3386-3398 (2014).
1036	24	Renner, L. D. & Weibel, D. B. Cardiolipin microdomains localize to negatively curved regions of Escherichia coli membranes. *Proceedings of the National Academy of Sciences of the United States of America* **108**, 6264-6269 (2011).
1039	25	Mileykovskaya, E. & Dowhan, W. Visualization of phospholipid domains in Escherichia coli by using the cardiolipin-specific fluorescent dye 10-N-nonyl acridine orange. *Journal of bacteriology* **182**, 1172-1175 (2000).
1042	26	Laloux, G. & Jacobs-Wagner, C. How do bacteria localize proteins to the cell pole? *J Cell Sci* **127**, 11-19 (2014).
1044	27	Lugtenberg, E. J. & Peters, R. Distribution of lipids in cytoplasmic and outer membranes of Escherichia coli K12. *Biochim Biophys Acta* **441**, 38-47 (1976).
1046	28	Onufryk, C., Crouch, M. L., Fang, F. C. & Gross, C. A. Characterization of six lipoproteins in the sigmaE regulon. *J Bacteriol* **187**, 4552-4561 (2005).
1048	29	Yan, Z., Hussain, S., Wang, X., Bernstein, H. D. & Bardwell, J. C. A. Chaperone OsmY facilitates the biogenesis of a major family of autotransporters. *Mol Microbiol* **112**, 1373-1387 (2019).
1051	30	Typas, A. *et al.* High-throughput, quantitative analyses of genetic interactions in E. coli. *Nat Methods* **5**, 781-787 (2008).
1053	31	Wu, T. *et al.* Identification of a multicomponent complex required for outer membrane biogenesis in Escherichia coli. *Cell* **121**, 235-245 (2005).
1055	32	Hagan, C. L., Kim, S. & Kahne, D. Reconstitution of outer membrane protein assembly from purified components. *Science* **328**, 890-892 (2010).
1057	33	Gunasinghe, S. D. *et al.* The WD40 Protein BamB Mediates Coupling of BAM Complexes into Assembly Precincts in the Bacterial Outer Membrane. *Cell Rep* **23**, 2782-2794 (2018).
1060	34	Knowles, T. J., Scott-Tucker, A., Overduin, M. & Henderson, I. R. Membrane protein architects: the role of the BAM complex in outer membrane protein assembly. *Nat Rev Microbiol* **7**, 206-214 (2009).
1063	35	Rojas, E. R. *et al.* The outer membrane is an essential load-bearing element in Gram-negative bacteria. *Nature* **559**, 617-621 (2018).
1065	36	Giuliani, M. M. *et al.* A universal vaccine for serogroup B meningococcus. *Proc Natl Acad Sci U S A* **103**, 10834-10839 (2006).
1067	37	Pizza, M. *et al.* Identification of vaccine candidates against serogroup B meningococcus by whole-genome sequencing. *Science* **287**, 1816-1820 (2000).
1069	38	Punta, M. *et al.* The Pfam protein families database. *Nucleic Acids Res* **40**, D290-301 (2012).
1071	39	Finn, R. D., Clements, J. & Eddy, S. R. HMMER web server: interactive sequence similarity searching. *Nucleic Acids Res* **39**, W29-37 (2011).

1073 40   Enright, A. J., Van Dongen, S. & Ouzounis, C. A. An efficient algorithm for large-scale
1074   detection of protein families. *Nucleic Acids Res* **30**, 1575-1584 (2002).

1075 41   Hunter, S. *et al.* InterPro in 2011: new developments in the family and domain
1076   prediction database. *Nucleic Acids Res* **40**, D306-312 (2012).

1077 42   Frickey, T. & Lupas, A. CLANS: a Java application for visualizing protein families based
1078   on pairwise similarity. *Bioinformatics* **20**, 3702-3704 (2004).

1079 43   Baba, T. *et al.* Construction of Escherichia coli K-12 in-frame, single-gene knockout
1080   mutants: the Keio collection. *Mol Syst Biol* **2**, 2006.0008 (2006).

1081 44   Datsenko, K. A. & Wanner, B. L. One-step inactivation of chromosomal genes in
1082   Escherichia coli K-12 using PCR products. *Proc Natl Acad Sci U S A* **97**, 6640-6645
1083   (2000).

1084 45   Kikuchi, S., Shibuya, I. & Matsumoto, K. Viability of an Escherichia coli pgsA null
1085   mutant lacking detectable phosphatidylglycerol and cardiolipin. *J Bacteriol* **182**, 371-
1086   376 (2000).

1087 46   Suzuki, M., Hara, H. & Matsumoto, K. Envelope disorder of Escherichia coli cells
1088   lacking phosphatidylglycerol. *J Bacteriol* **184**, 5418-5425 (2002).

1089 47   Browning, D. F. *et al.* Laboratory adapted Escherichia coli K-12 becomes a pathogen
1090   of Caenorhabditis elegans upon restoration of O antigen biosynthesis. *Mol Microbiol*
1091   **87**, 939-950 (2013).

1092 48   Browning, D. F. *et al.* Mutational and Topological Analysis of the Escherichia coli
1093   BamA Protein. *PLoS One* **8**, e84512 (2013).

1094 49   Isom, G. L. *et al.* MCE domain proteins: conserved inner membrane lipid-binding
1095   proteins required for outer membrane homeostasis. *Sci Rep* **7**, 8608 (2017).

1096 50   Dalebroux, Z. D. *et al.* Delivery of cardiolipins to the Salmonella outer membrane is
1097   necessary for survival within host tissues and virulence. *Cell Host Microbe* **17**, 441-
1098   451 (2015).

1099 51   Bligh, E. G. & Dyer, W. J. A rapid method of total lipid extraction and purification. *Can
1100   J Biochem Physiol* **37**, 911-917 (1959).

1101 52   Wu, H., Southam, A. D., Hines, A. & Viant, M. R. High-throughput tissue extraction
1102   protocol for NMR- and MS-based metabolomics. *Anal Biochem* **372**, 204-212 (2008).

1103 53   Teo, A. C. K. *et al.* Analysis of SMALP co-extracted phospholipids shows distinct
1104   membrane environments for three classes of bacterial membrane protein. *Sci Rep* **9**,
1105   1813 (2019).

1106 54   Parham, N. J. *et al.* PicU, a second serine protease autotransporter of uropathogenic
1107   *Escherichia coli*. *FEMS Microbiol Lett* **230**, 73-83 (2004).

1108 55   Leyton, D. L. *et al.* Size and conformation limits to secretion of disulfide-bonded
1109   loops in autotransporter proteins. *J Biol Chem* **286**, 42283-42291 (2011).

1110 56   Selkrig, J. *et al.* Discovery of an archetypal protein transport system in bacterial outer
1111   membranes. *Nat Struct Mol Biol* **19**, 506-510, S501 (2012).

1112 57   Knowles, T. J. *et al.* Structure and function of BamE within the outer membrane and
1113   the beta-barrel assembly machine. *EMBO Rep* **12**, 123-128 (2011).

1114 58   Wisniewski, J. R., Zougman, A., Nagaraj, N. & Mann, M. Universal sample preparation
1115   method for proteome analysis. *Nat Methods* **6**, 359-362 (2009).

1116 59   Muhandiram, D. R. & Kay, L. E. Gradient-enhanced triple resonance three-
1117   dimensional NMR experiments with improved sensitivity. . *J Magn Reson* **B103**, 203-
1118   216 (1994).

1119 60 Delaglio, F. *et al.* NMRPipe: a multidimensional spectral processing system based on
1120   UNIX pipes. *Journal of biomolecular NMR* **6**, 277-293 (1995).
1121 61 Goddard, T. D. & Kneller, D. G. SPARKY 3. *University of California San Francisco*
1122   (2008).
1123 62 Cornilescu, G., Delaglio, F. & Bax, A. Protein backbone angle restraints from
1124   searching a database for chemical shift and sequence homology. *Journal of*
1125   *biomolecular NMR* **13**, 289-302 (1999).
1126 63 Schanda, P., Kupce, E. & Brutscher, B. SOFAST-HMQC experiments for recording two-
1127   dimensional heteronuclear correlation spectra of proteins within a few seconds.
1128   *Journal of biomolecular NMR* **33**, 199-211 (2005).
1129 64 Guntert, P. Automated NMR structure calculation with CYANA. *Methods in molecular*
1130   *biology* **278**, 353-378 (2004).
1131 65 Linge, J. P., O'Donoghue, S. I. & Nilges, M. Automated assignment of ambiguous
1132   nuclear overhauser effects with ARIA. *Methods in enzymology* **339**, 71-90 (2001).
1133 66 Laskowski, R. A., Moss, D. S. & Thornton, J. M. Main-chain bond lengths and bond
1134   angles in protein structures. *J Mol Biol* **231**, 1049-1067 (1993).
1135 67 Koradi, R., Billeter, M. & Wuthrich, K. MOLMOL: a program for display and analysis of
1136   macromolecular structures. *Journal of molecular graphics* **14**, 51-55, 29-32 (1996).
1137 68 Dancea, F., Kami, K. & Overduin, M. Lipid interaction networks of peripheral
1138   membrane proteins revealed by data-driven micelle docking. *Biophys J* **94**, 515-524
1139   (2008).
1140 69 Konarev, P. V. *et al.* PRIMUS - a Windows-PC based system for small-angle scattering
1141   data analysis. *J Appl Cryst.* **36**, 1277-1282 (2003).
1142 70 Guinier, A. La diffraction des rayons X aux tres petits angles; applicationa l'etude de
1143   phenomenes ultramicroscopiques. *Ann. Phys.* **12**, 161-237 (1939).
1144 71 D.I., S. Determination of the regularization parameter in indirect-transform methods
1145   using perceptual criteria. . *J. Appl. Crystallogr.* **25**, 495-503 (1992).
1146 72 Franke, D. & Svergun, D. I. DAMMIF, a program for rapid ab-initio shape
1147   determination in small-angle scattering. *J Appl Crystallogr* **42**, 342-346 (2009).
1148 73 Volkov, V. V. & Svergun, D. I. Uniqueness of ab-initio shape determination in small-
1149   angle scattering. *J. Appl. Cryst.* **36**, 860-864 (2003).
1150 74 Bernado, P., Perez, Y., Svergun, D. I. & Pons, M. Structural characterization of the
1151   active and inactive states of Src kinase in solution by small-angle X-ray scattering. *J*
1152   *Mol Biol* **376**, 492-505 (2008).
1153 75 Petoukhov, M. V. & Svergun, D. I. Global rigid body modeling of macromolecular
1154   complexes against small-angle scattering data. *Biophys J* **89**, 1237-1250 (2005).
1155 76 Ducret, A., Quardokus, E. M. & Brun, Y. V. MicrobeJ, a tool for high throughput
1156   bacterial cell detection and quantitative analysis. *Nat Microbiol* **1**, 16077 (2016).
1157 77 Banzhaf, M. *et al.* Outer membrane lipoprotein NlpI scaffolds peptidoglycan
1158   hydrolases within multi-enzyme complexes in Escherichia coli. *EMBO J* **39**, e102246
1159   (2020).
1160 78 Kritikos, G. *et al.* A tool named Iris for versatile high-throughput phenotyping in
1161   microorganisms. *Nat Microbiol* **2**, 17014 (2017).
1162 79 Chong, Z. S., Woo, W. F. & Chng, S. S. Osmoporin OmpC forms a complex with MlaA
1163   to maintain outer membrane lipid asymmetry in Escherichia coli. *Molecular*
1164   *microbiology* **98**, 1133-1146 (2015).

1165   80   Yim, H. H. & Villarejo, M. *osmY*, a new hyperosmotically inducible gene, encodes a
1166   periplasmic protein in *Escherichia coli*. *J Bacteriol* **174**, 3637-3644 (1992).
1167   81   Weber, A., Kogl, S. A. & Jung, K. Time-dependent proteome alterations under
1168   osmotic stress during aerobic and anaerobic growth in *Escherichia coli*. *J Bacteriol*
1169   **188**, 7165-7175 (2006).
1170   82   Ashraf, K. U. *et al.* The Potassium Binding Protein Kbp Is a Cytoplasmic Potassium
1171   Sensor. *Structure* **24**, 741-749 (2016).
1172   83   Lennon, C. W. *et al.* Folding Optimization In Vivo Uncovers New Chaperones. *Journal*
1173   *of molecular biology* **427**, 2983-2994 (2015).
1174   84   Li, L. *et al.* DelPhi: a comprehensive suite for DelPhi software and associated
1175   resources. *BMC Biophys* **4**, 9 (2012).
1176   85   Moseley, H. N., Sahota, G. & Montelione, G. T. Assignment validation software suite
1177   for the evaluation and presentation of protein resonance assignment data. *J Biomol*
1178   *NMR* **28**, 341-355 (2004).
1179   86   Bhattacharya, A., Tejero, R. & Montelione, G. T. Evaluating protein structures
1180   determined by structural genomics consortia. *Proteins* **66**, 778-795 (2007).
1181

Figure 1

A

lpoA *yraN* σ^E σ^E *diaA* *dolP*

3291422 3295006

DolP BON BON
19 53 112 130 190

OsmY BON BON
28 60 123 139 201

Kbp BON LysM
28 91 99 149

B

Kbp

OsmY

DolP

C

E. coli BW25113

WT

△*dolP*

COMP

VAN SDS

D

10^-2 10^-3 10^-4 10^-5 10^-6 10^-7

WT pET17b
△*dolP* pET17b
△*dolP* pSe
△*dolP* pVc
△*dolP* pNm
△*dolP* pHi
△*dolP* pOsmY
△*dolP* pPm

Figure 1-figure supplement 1

A

WT △*dolP* COMP

DolP
BamC
BamE

B

WT △*dolP* C19A COMP

BamB
DolP

C

- - + + - - + + Trypsin
- + - + - + - + Polymyxin B

DolP
SurA
RNAP

WT   △*dolP*

D

	Fixed cells				Permeabilised cells		
	WT	△*dolP*	COMP		WT	△*dolP*	COMP
Anti-DolP							
Anti-SurA							

Figure 1-figure supplement 2

Figure 1-figure supplement 3

A

E. coli BW25113

WT
△dolP
osmY::aph
kbp::aph

VAN   SDS

B

VAN   SDS

WT

△dolP

△dolP
p(OM)OsmY

C

| | WT C1 | WT C2 | △dolP C1 | △dolP C2 | osmY::aph C1 | osmY::aph C2 | kbp::aph C1 | kbp::aph C2 |

10^{-2}
10^{-3}
10^{-4}
10^{-5}
10^{-6}
10^{-7}

NaCl   0 mM   400 mM   600 mM   800 mM

Figure 1-figure supplement 4

A

Cholate 2% Deoxycholate 2% LB

B

C

WT

2μm

△dolP

2μm

Figure 1-figure supplement 5

DolP

BON   BON

19   53   112 130   190

DolP^{IM}   MKALSPIAVLISALLLQGC**DD**AAV   **+2/3**
DolP^{WT}   MKALSPIAVLISALLLQGC**VA**AAV
19

DolP^{WT}   DolP^{WT}

DolP^{IM}   DolP^{IM}

DolP^{pelB}   DolP^{pelB}

BW25113   Δ*dolP*

4.8 % SDS

LB

Δ*dolP*

DolP-mCherry

DolP

Figure 2

A

α1 β1 β2 β3 α1* α2

α4 β6 β4 β5 α3

BON1   BON2

62 67
60   α1'
α1
70
47
Nt
75 78
β1 β2
82
88
α2
99
106
β3
111
120

152
α3
138 148
155
α4
159
176
β5
164
β6
182
185
Ct

B

C19

S²
1.0
0.8
0.6
0.4
0.2
0.0
50   100   150   200
Residue No.

C

χ²=1.263

Log(I)
100
10
1
0.1
0.01
0.001
0.0 0.1 0.2 0.3 0.4 0.5
s (Å⁻¹)

D

△dolP

DolP WT EV Y75A G83V G160V G83V; G160V

BamB
DolP

10⁻²
10⁻³
10⁻⁴
10⁻⁵
10⁻⁶
10⁻⁷

E

V72 L50
A88 V54
Q113 N105
N109
Q76
D125 G160
W127 L136 L142

△dolP

DolP WT EV L50 V54 V72 Q76 A88 D102 N105 N109 Q113 D125 W127 L136 V142 G160

BamB
DolP

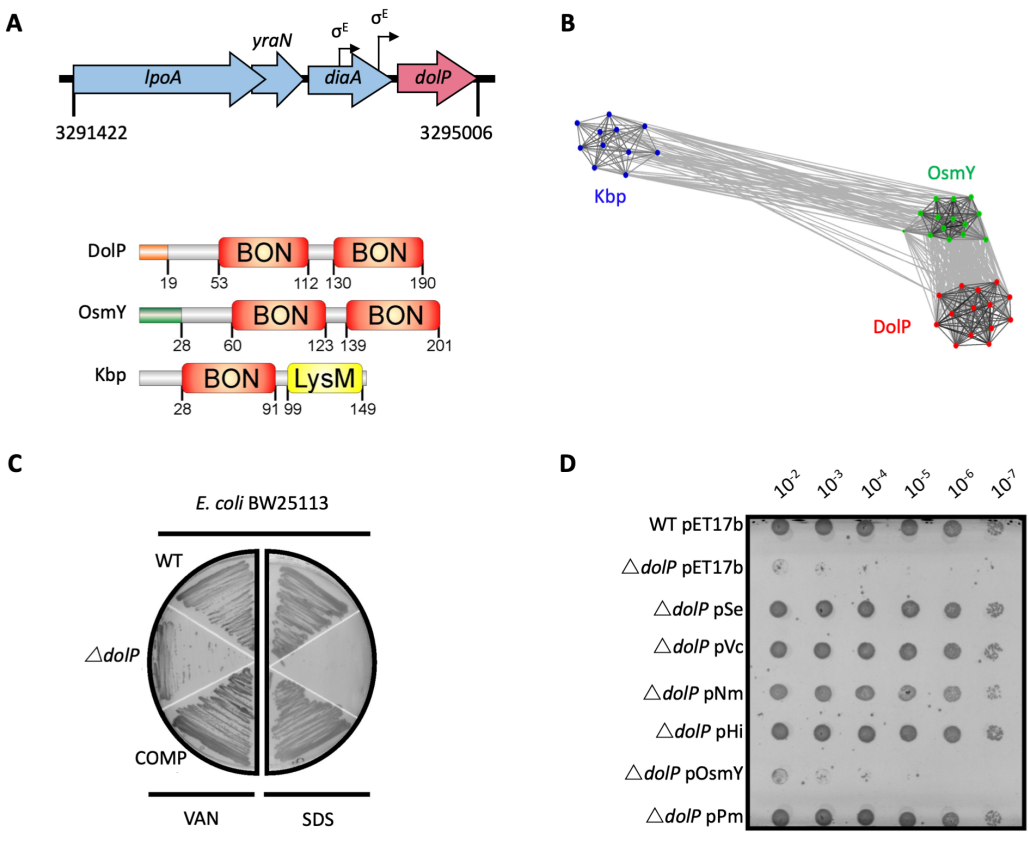10⁻²
10⁻³
10⁻⁴
10⁻⁵
10⁻⁶
10⁻⁷

Figure 2-figure supplement 1

Figure 2-figure supplement 2

Figure 2-figure supplement 3

A

```
                    10        20        30        40        50        60        70
          ....|....|....|....|....|....|....|....|....|....|....|....|....|....|....|
BON2_DolP         LGEASNDTWITTKVRSQLLTSDLVKSSN-VKVTTENGEVFLMGLVT-EREAKAAADIASRVSGVKRVTTAFTFIK
BON1_DolP         VGTQVDDGTLEVRVNSALSKDEQIKKEARINVTAYQGKVLLVGSQPNAELSARAKQIAMGVDGANEVYNEIRQGQ
OsmY_BON1         VGNFMDDSAITAKVKAALVDHDNIKSTD-ISVKTDQKVVTLSGFVESQAQAEEAVKVAKGVEGVTSVSDKLHVRD
OsmY_BON2         VKGYAGDTATTSEIKAKLLADDIVPSRH-VKVETTDGVVQLSGTVDSQAQSDRAESIAKAVDGVKSVKNDLKTK-
Kbp_BON           VTGQHDKDDQAKKVQEHLNKTG-IPDADKVNIQIADGKATVTGDGLSQEAKEKILVAVGNISGIASVDDQVKTAT
OmpATB_BON        IHVDPVVRSLDFSSAEPVFTAS-VPIPD-FGLKVERDTVTLTGTAPSSEHKDAVKRAATSTWPDMKIVNNIEVTG
Clustal Consensus         :          :       :   .: .      .  : *       .     .      :  : .
```


B

```
                    10        20        30        40        50        60        70        80        90       100
          ....|....|....|....|....|....|....|....|....|....|....|....|....|....|....|....|....|....|....|....|
E. coli_DolP         -----------MKALSPIAVLIS-ALLLQGCVAAAVVGTAAVGTKAATDPRSVGTQVDDGT--LEVRVNSALS---KDEQIKKEARINVTAYQGKVLLV
S. enterica_DolP     -----------MKAFSPLAVLIS-ALLLQGCVAAAVVGTAAVGTKAATDPRSVGTQVDDGT--LELRVSSALS---KDEQIKKETRINVTAYQGKVLLV
V. cholerae_DolP     -----------MKSIRLLIVSGLLA-TLTGCAGLFIAG-AATTANIVTDPRSTQEIWQDNNVELEVAGLA------NKEPYRKDARISAVAYRGTVVLL
N. meningitidis_DolP -----------MKFKPHTVRTLIAAIFSLALSGGCVSAVI-GSAAVGAKSAVDRRTTGAQTDDNVMALRIETTARSYLRQNNQTKGTTPQISVVGYNRHLLLL
H. influenzae_DolP   -----------MTLSPLKKLAILLGATIFLQGCVAA-VIGGGAVAAKVATDPRTTGTQIDDET--LEFKVENAVE----KDAQIKAEGRVNAVSYNGRVLLS
E. coli_OsmY         MTMTRLKISKTLLAVMLTSAVATGSAYAEN----NAQTTNESAGQKVDSSMNKVGNFMDDSAITAKVKAALV-----DHENIKSTD-ISVKTDQKVVTLS
C. rodentium_OsmY    MTMTRLKISKTLLAVMLTSAVATGSAYAENSTTDKAQAGAESAGQKVDSSMNKVGNFMDDSAITAKVKAALV-----DHENIKSTD-ISVETNQKVVTLS
S. enterica_OsmY     MTMTRLKISKTLLAVMLTSAVATGSAFAENATTDKAQSGTETAGQKVDSSMNKVGNFMDDSAITAKVKAALV-----DHDNIKSTD-ISVKTDQKVVTLS
E. cloacae_OsmY      MNMTRLKISKTLLAVTLGSVLVSGSALAESSTMDKAQSTADSAGQKIDSSMNKVGNFMDDSITAKVKAALV-----DDEAIKSTD-ISVKTDKKVVTLS
K. pneumoniae_OsmY   --MTRLKNANMLLALFLGLAALNASAETEKTTVDSAKSAASNAGEAVDNSINKVGDFMDDSTITARVKAALI-----DHKDINSGD-ISVKTENKVVTLS
Clustal Consensus                  .              .  .  ....   .*.:.:*   . : :     . .: .:             :*  .:     *
```

BON1

```
                    110       120       130       140       150       160       170       180       190       200
          ....|....|....|....|....|....|....|....|....|....|....|....|....|....|....|....|....|....|....|....|
E. coli_DolP         GSQPNAELSARAKQIAMGVDGANEVYNEIRQGQ-----PIGLGEASNDTWITTKVRSQLLTSDLVKSSNVKVTTENGEVFLMGLVTER-EAKAAADIASR
S. enterica_DolP     GSQPNSELSARAKQIAMGVEGTTEVYNEIRQGQ-----PIGLGTASNDTWITTKVRSQLLTSDQVKSSNVKVTTENGEVFLLGLVTER-EGKAAADIASR
V. cholerae_DolP     GSQRNEAILEQFIAQARQLKGVKELHNQVQIK-----APLSVGEISNDSWITTKVKSALLTKSELNGIKIKVVTEDRVVYLFGYVSPE-HAEMAIGVARN
N. meningitidis_DolP GQVATEGEKQFVGQIARSEQAAEGVTNYITVAS----LPRTAGDIAGDTWNTSKVRATLLGISPATQARVKIVTYGNVTYVMGILTPE-EQAQITQKVST
H. influenzae_DolP   GQVPNSDVKDTATALAKGVEGVNEVTNELTVSP-----KISFAQISKDSWLTQVKSKMFVDGRVKATDVKVISENGEVFLLGNVTQS-QANAAADIASK
E. coli_OsmY         GFVESQAQAEEAVKVAKGVEGVTSVSDKLHVRD----AKEGSVKGYAGDTATTSEIKAKLLADDIVPSRHVKVETTDGVVQLSGTVDSQAQSDRAESIAKA
C. rodentium_OsmY    GFVESQAQAEEAVKVAKGVEGVTSVSDKLHVRD-----DHEGSVKGYAGDTATTSEVKAKLLADDIVPSRKVKVETTDGVVQLSGTVDSQAQIDRAESIAKA
S. enterica_OsmY     GFVESQAQAEEAVKVAKGIEGVTSVSDKLHVRD-----NKEGSVKGYAGDTATTSEVKAKLLADDIVPSRKVKVETTDGVVQLSGTVETQEQSDRAESIAKA
E. cloacae_OsmY      GFVESQAQAEQAVKVAKGVSAVSVSDKLHVRD-----GKNASVKGYAGDAATTSEIKAKLLADDIVPSRKVKVETTDGVVQLSGTVDSQAQSERAEAIAKA
K. pneumoniae_OsmY   GDVTSAEQKSQALSVAKEVKGVSHVNDKLTVHHKSSSETATLKGYAGDTAITSEVKAKLLADDIVPSRNVKVETTNAGAVHLTGTVASAAQAERAAEIAKA
Clustal Consensus    *          *              .       .    : .   :*  *:.:::::  . :    :*:   : *    :      . *    ::  * .
```

BON2

```
                    210
          ....|....|....|..
E. coli_DolP         VSGVKRVTTAFT-FIK-
S. enterica_DolP     VSGVKRVTTAFT-YIK-
V. cholerae_DolP     IIGVKQVVKAFD-YAQ-
N. meningitidis_DolP TVGVQKVITLTQNYVQR
H. influenzae_DolP   ISGVKKVIKVFK-YLD-
E. coli_OsmY         VDGVKSVKNDLKTK---
C. rodentium_OsmY    VDGVKSVKNDLKAK---
S. enterica_OsmY     VDGVKSVKNDLKVQ---
E. cloacae_OsmY      IDGVKSVKNDLKTK---
K. pneumoniae_OsmY   VSGVKSVRNDLSVK---
Clustal Consensus    **: . *    .
```
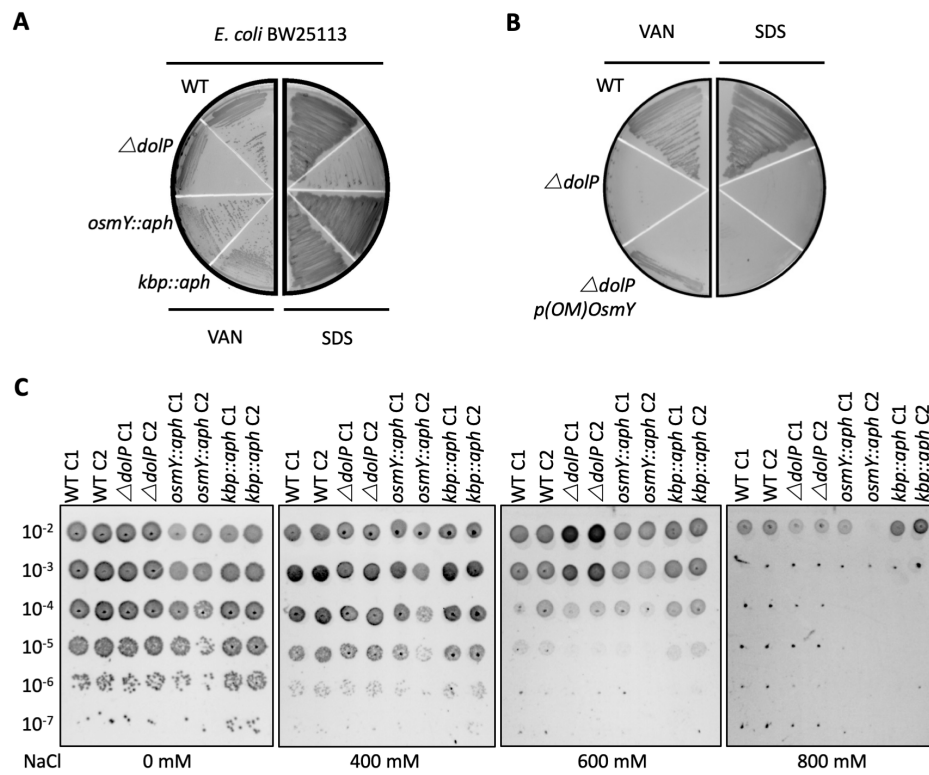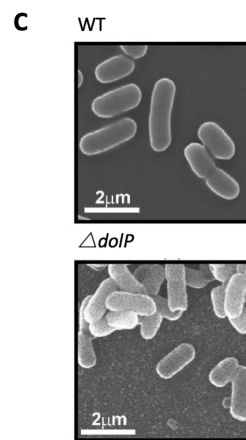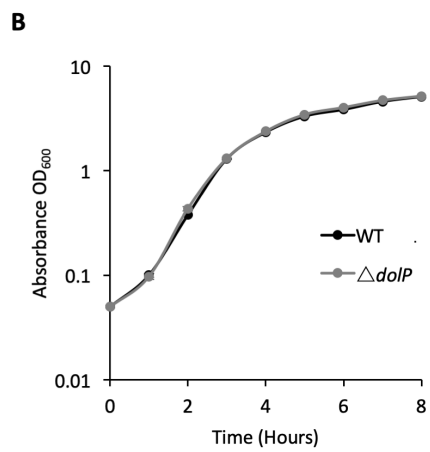
Figure 2-figure supplement 4

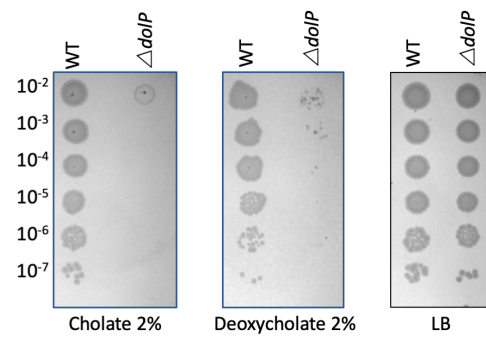**Figure 2-figure supplement 5**

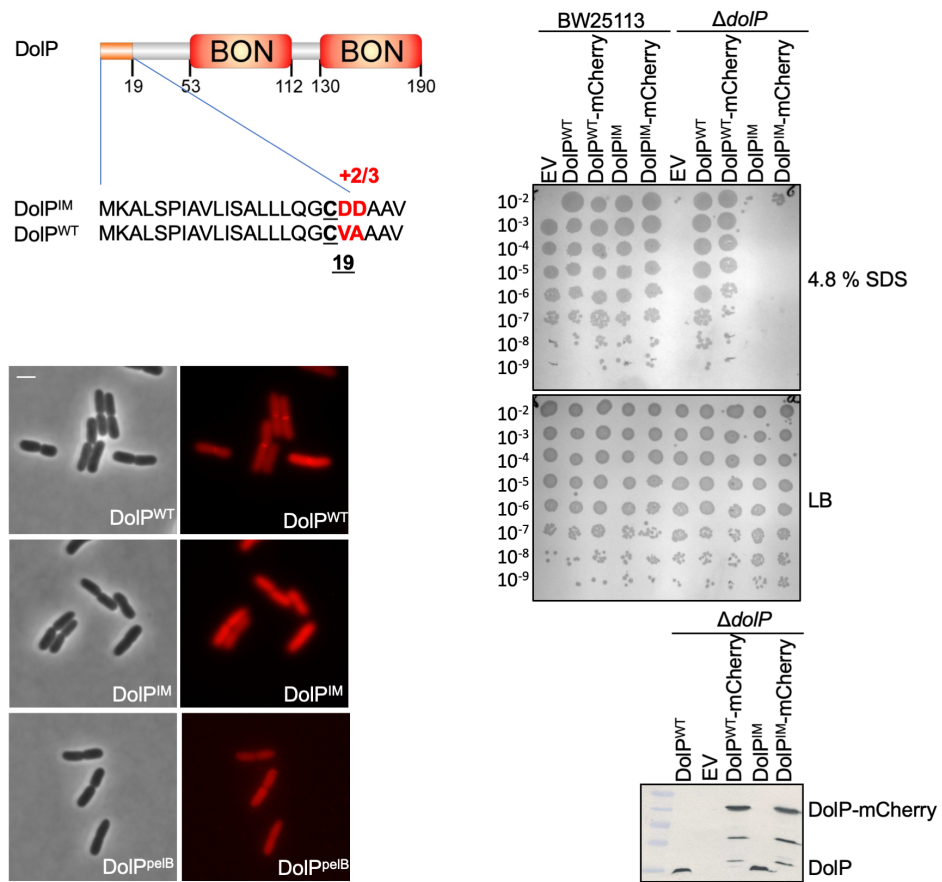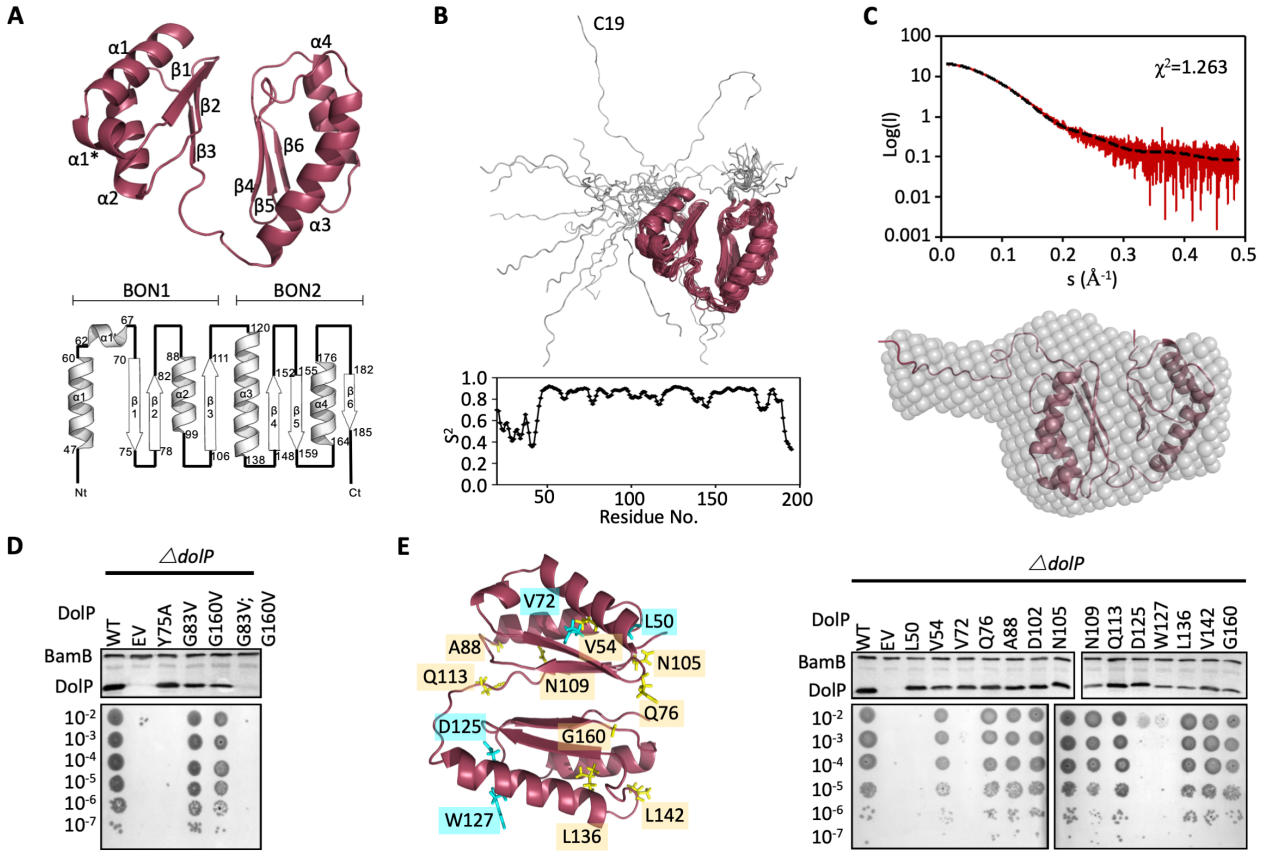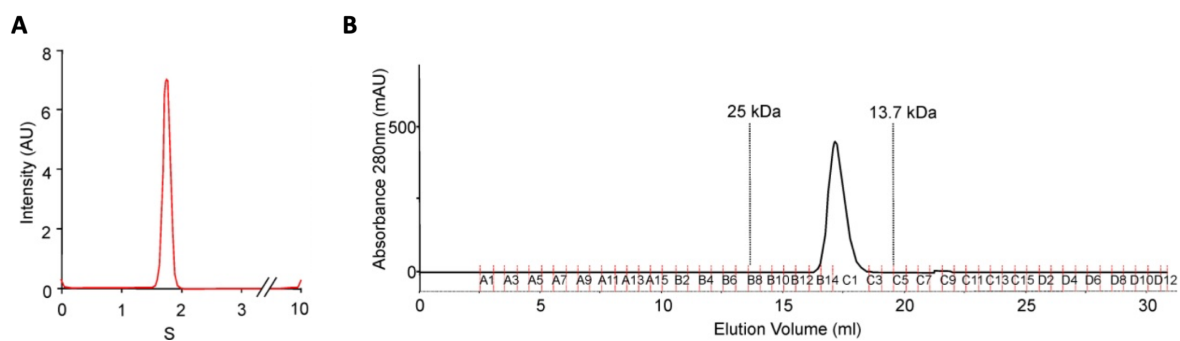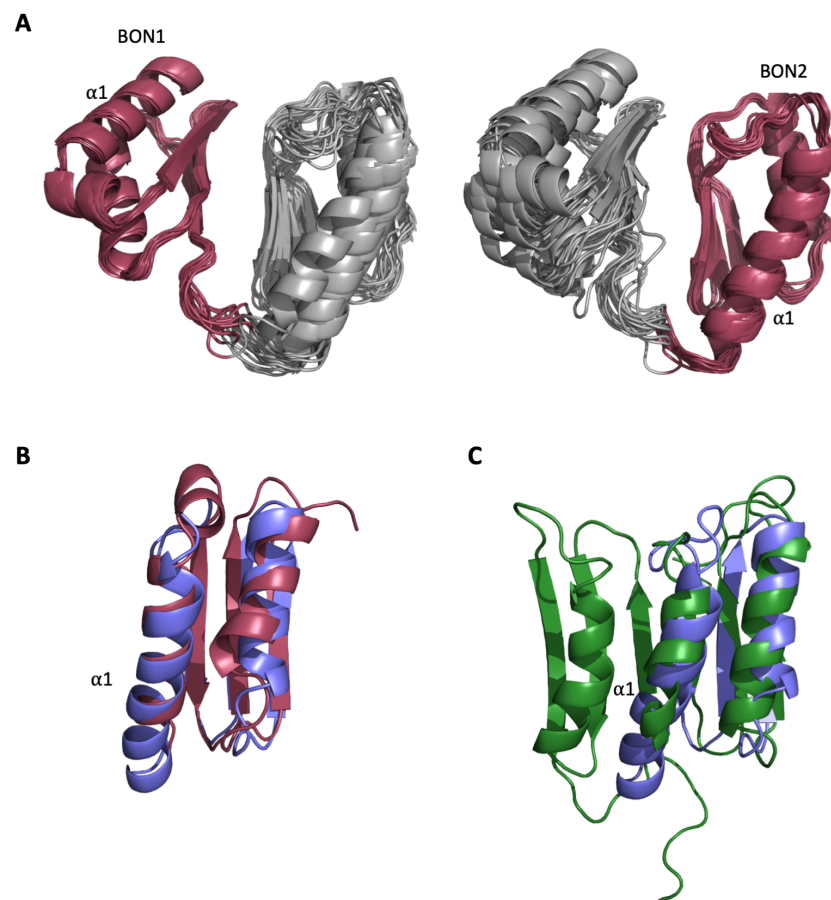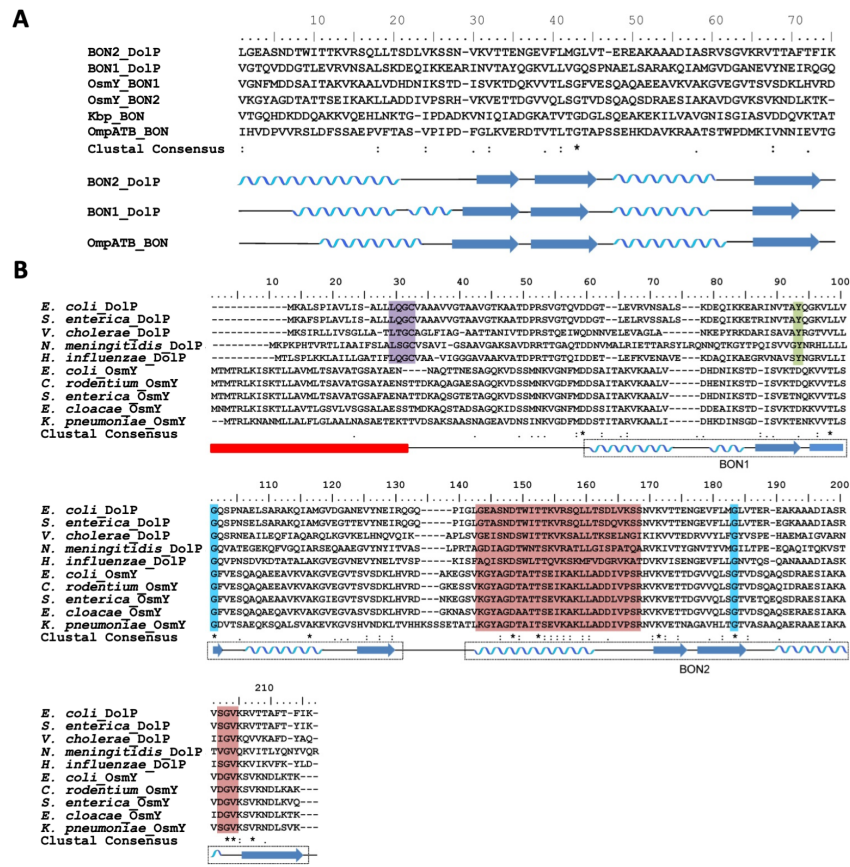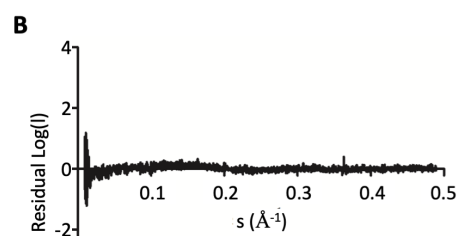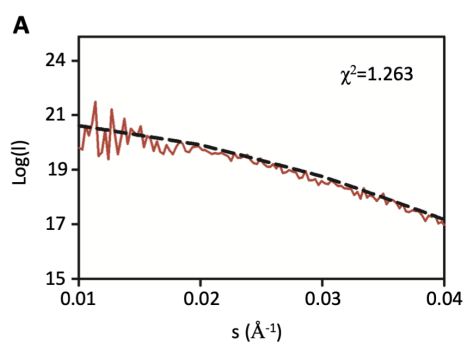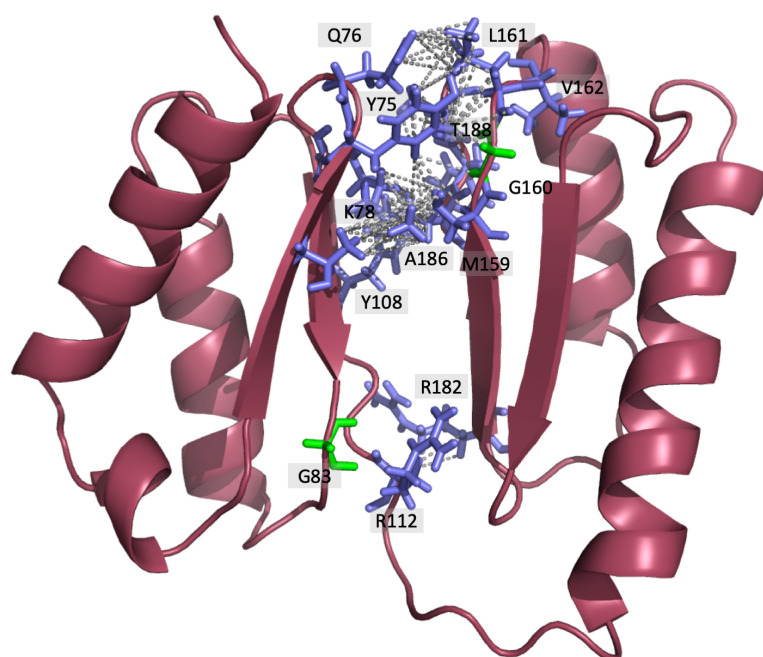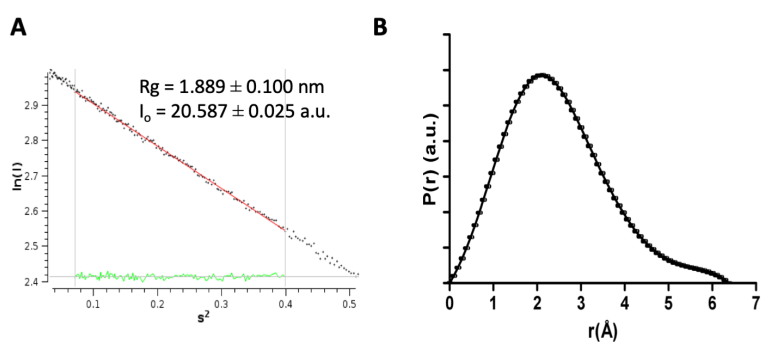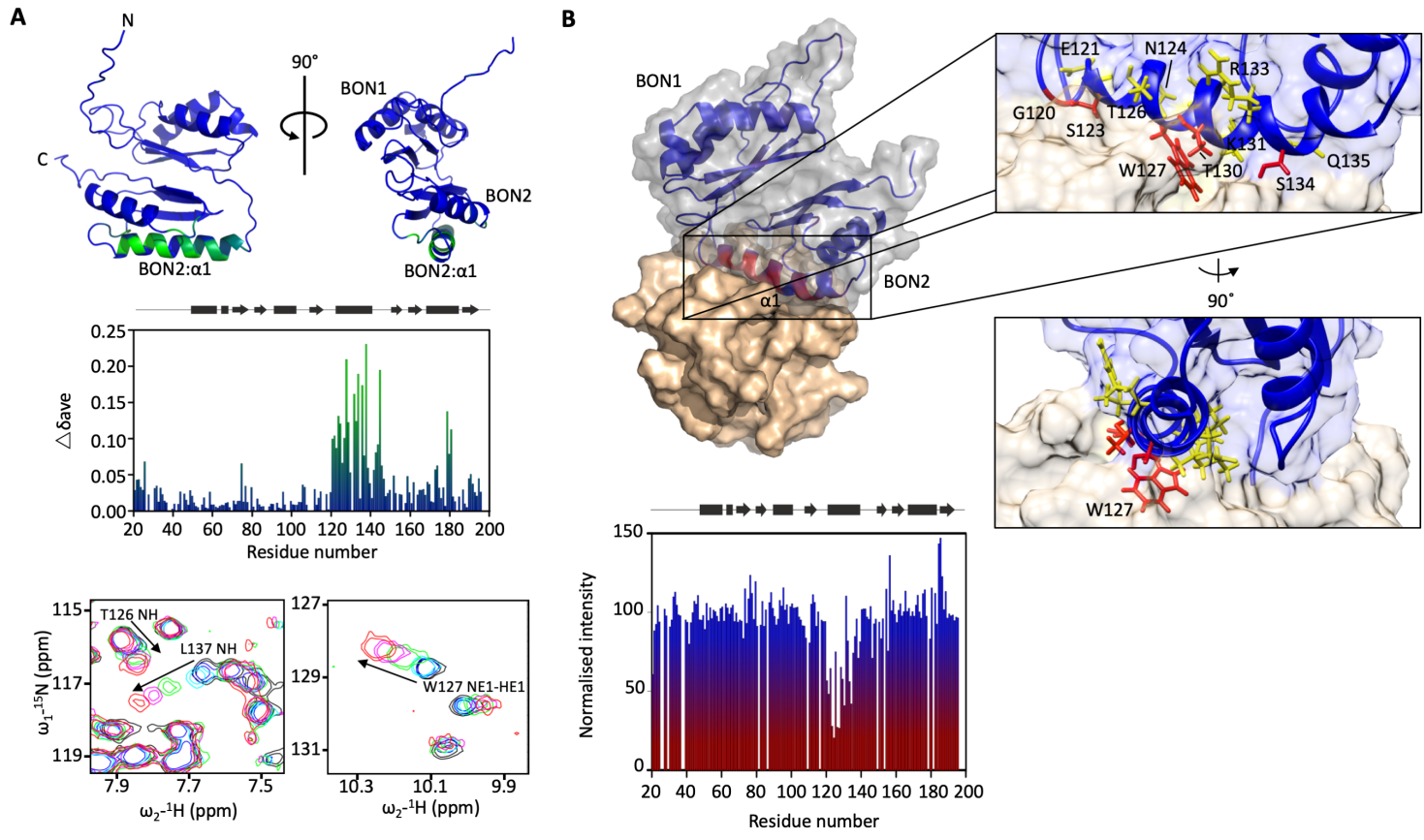**Figure 2-figure supplement 6**

A

Rg = 1.889 ± 0.100 nm
I_o = 20.587 ± 0.025 a.u.

ln(I)

2.9
2.8
2.7
2.6
2.5
2.4

0.1   0.2   0.3   0.4   0.5

s^2

B

P(r) (a.u.)

0   1   2   3   4   5   6   7

r(Å)

Figure 3

Figure 3-figure supplement 1

A

Fitness ratios of double mutants:

Observed: $\dfrac{\Delta dolP \Delta bam}{WT}$

Expected: $\dfrac{\Delta dolP}{WT} \times \dfrac{\Delta bam}{WT}$

fitness ratio

dolP genetic interaction pair

☐ *bam*   ☐ *dolP*   ☐ double expected   ■ double observed

B

WT   △*dolP*

△*bamB*   △*dolP* △*bamB*

△*bamC*   △*dolP* △*bamC*

△*bamE*   △*dolP* △*bamE*

C

△*dolP*   WT

EV   DolP   BamA

BamA
BamB
BamC
DolP—
BamD
BamE

D

n   d
WT △*dolP*   WT △*dolP*

250
180
130
95
72
55
43
34
26

Coomassie

Figure 3-figure supplement 2

A

WT   ΔdolP   COMP   WT   ΔdolP   COMP

pet20b-*wbbL*   pet20b-

B

IM   OM

WT   ΔdolP   WT   ΔdolP

Solvent front

CL

PG
PE

Origin

IM phospholipids

OM phospholipids

Relative abundance

Phospholipid classes

lysoPE   PE   PG   CL

WT   ΔdolP

C

Strain   Parent   ΔdolP   Parent   ΔmlaA

DolP   EV   EV   EV   DolP   DolP   EV

Lipid A
4-monophosphate
Hepta-acyl
Hexa-acyl
1-pyrophosphate

Origin

Lipid A palmitoylation (%)

NS

DolP   EV   EV   EV   DolP   DolP   EV
Strain   Parent   ΔdolP   Parent   ΔmlaA

D

Membrane fluidity

WT   ΔdolP   ΔwaaD

Figure 3-figure supplement 3

A

300 μM DolP + 0mM PG
300 μM DolP + 40mM PG

B

Phosphatidylethanolamine (20mM)

Phosphatidylglycerol (40mM)

Figure 3-figure supplement 4

Figure 4

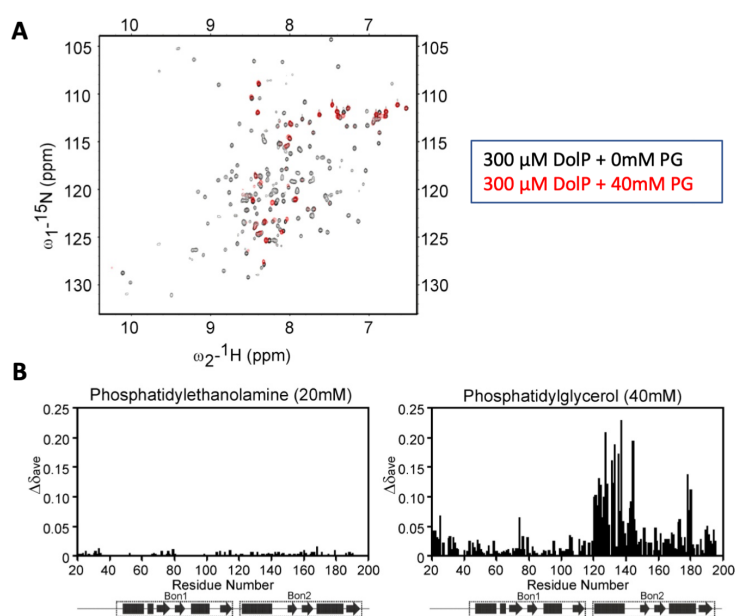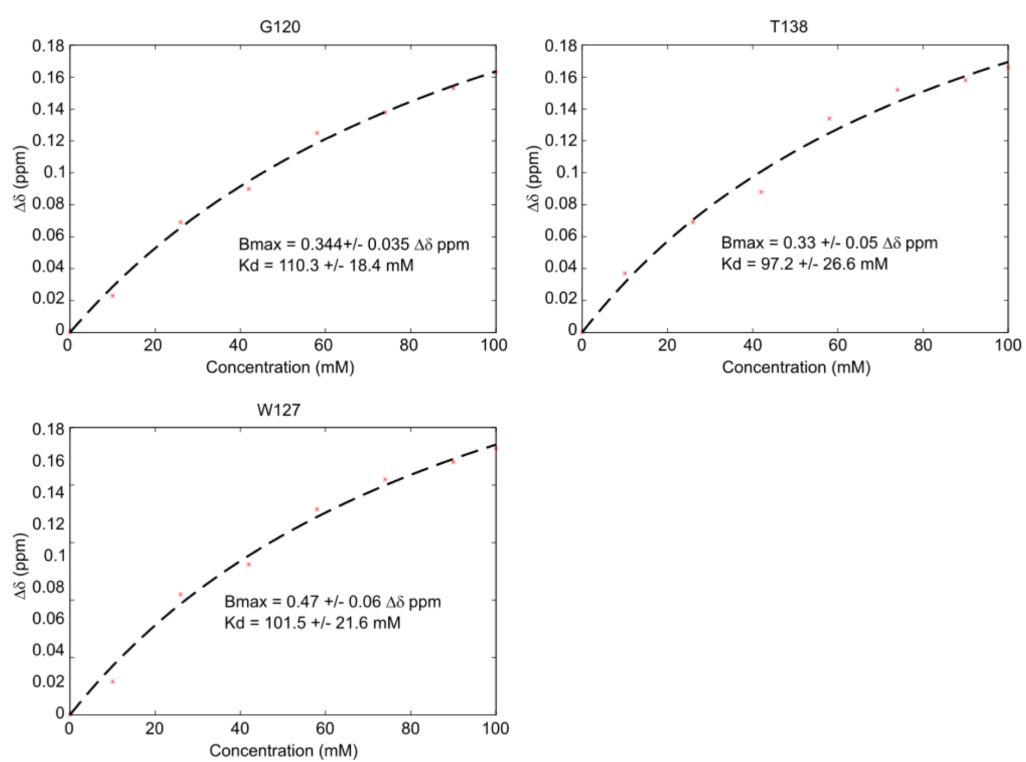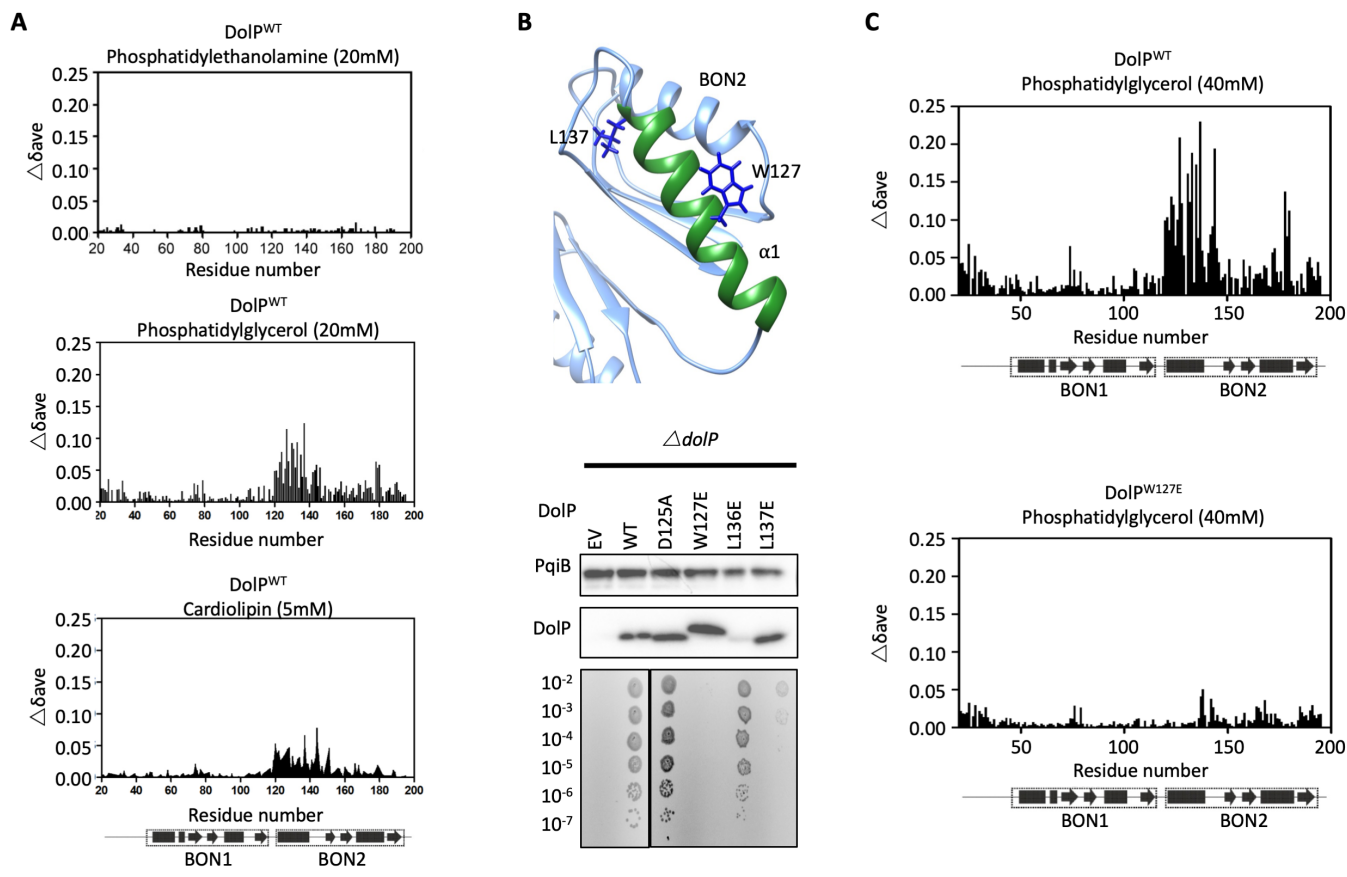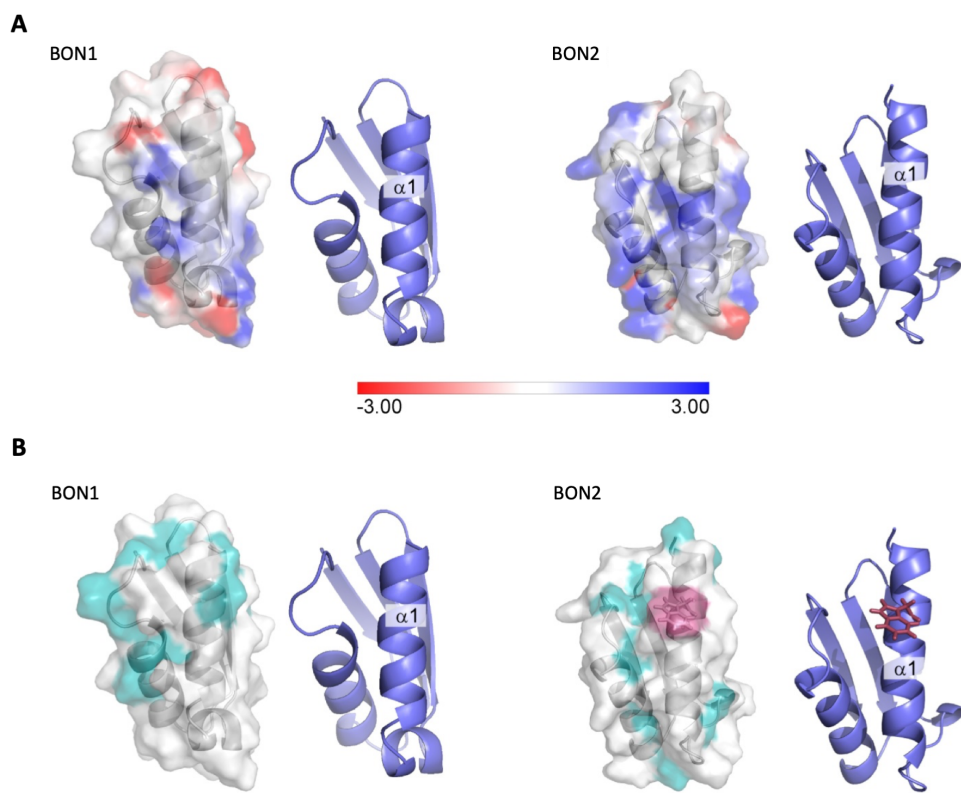**Figure 4-figure supplement 1**
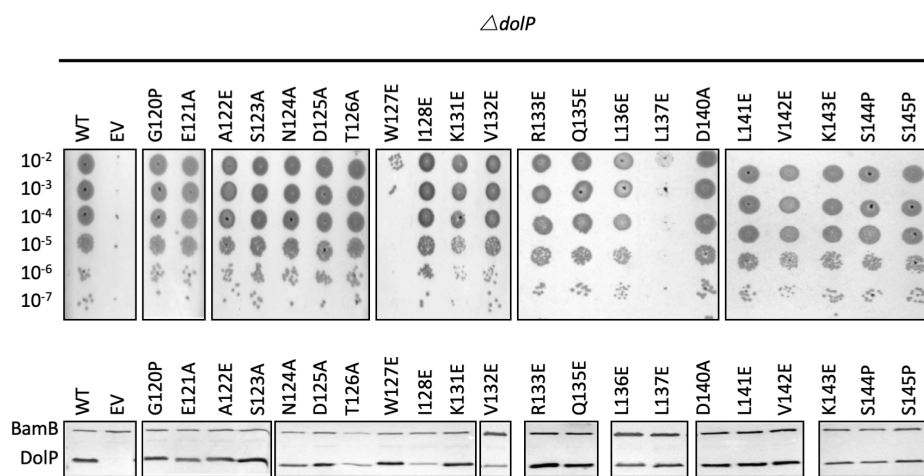
Figure 4-figure supplement 2

Figure 5

A

△*dolP* DolP^WT

△*dolP* DolP^W127E

△*dolP* DolP^WT

△*dolP* DolP^W127E

Relative position

3
2
1
0
-1
-2
-3

Cell length

△*dolP* DolP^WT

Cell length

△*dolP* DolP^W127E

Fluorescence intensity (AU)

60,000
50,000
40,000
30,000
20,000
10,000
0

B

SF

CL

PG

PE

Origin

WT

△*rcsF*,△*lpp*

△*pgsA*

△*clsABC*

C

WT DolP^WT

WT DolP^WT

△*pgsA* DolP^WT

△*pgsA* DolP^WT

△*clsABC* DolP^WT

△*clsABC* DolP^WT